Experimental analysis of longitudinal shear between the web and flanges of T-beams made of fibre-reinforced concrete.

Pereiro-Barceló, Javier[1]; López-Juárez, José Antonio[2]; Ivorra-Chorro, Salvador[3]; Bonet, José L.[4]

[1] Instituto Universitario de Investigación de Ciencia y Tecnología del Hormigón, Universitat Politècnica de València, Valencia, Spain C/Vera unnumbered, Valencia, 46022, Spain japebar@upv.es

[2] Departamento de Ingeniería Civil, Universidad Católica de Murcia, Campus de Los Jerónimos, Guadalupe 30107 (Murcia), Spain jalopez6@ucam.edu

[3] Departamento de Ingeniería Civil, Universitat d'Alacant, San Vicente del Raspeig Road unnumbered, Alicante, 03690, Spain sivorra@ua.es

[4] Instituto Universitario de Investigación de Ciencia y Tecnología del Hormigón (ICITECH), Universitat Politècnica de València, Vera Street unnumbered, Valencia, 46022, Spain jlbonet@cst.upv.es

ABSTRACT.

The longitudinal shear between the web and flanges of T-beams is an Ultimate Limit State contemplated by technical codes. For this reason, the longitudinal shear must be compared with the longitudinal shear resistance of the flange. Longitudinal shear strength can be increased by including steel fibres in the concrete mass. This article shows the experimental results of 13 T-beams mounted on two supports subjected to two central loads. Four of these beams were made with conventional concrete and nine with fibre-reinforced concrete. The direct instrumentation results are discussed and the failure process is described. Longitudinal shear cracking load is studied on the basis of both a theoretical approach and experimental results. An analysis is performed to evaluate each specimen's longitudinal shear, not only in the ultimate state, but also throughout the loading process evolution, based on load and strain records. This process involves determining each beam's effective width. The experimental data confirm an increase in longitudinal shear strength caused by adding steel fibres to concrete.

KEY WORDS:

Longitudinal shear strength; longitudinal shear cracking load; web-flange junctions; fibre-reinforced concrete; T-beams.

HIGHLIGHTS:

- 13 T-beams were tested to study the longitudinal shear strength of web-flange junctions.
- The inclusion of steel fibres improves longitudinal shear strength.
- Effective width depends on transversal reinforcement and steel fibre content.
- A procedure was developed to calculate longitudinal shear cracking load.
- Maximum web-flange longitudinal shear and bending moment situations may not match.

1. Introduction.

The use of reinforced concrete T-beams or double T-beams is widespread both in buildings and bridge decks due to their high flexural strength / weight ratio. The design codes [1,2] contemplate the longitudinal shear analysis between the web and flanges as a Ultimate Limit State in order to ensure the integral behaviour of the compressed wings against normal or tangential stresses. The web-flange tangential stress τ_{xy} is produced by the variation of the axial force N_f in the flange along a beam zone [1,2]. This tangential stress τ_{xy} is simultaneous with a flange normal stress σ_x and with a web-flange normal stress σ_y (Figure 1.a-b). The web-flange stress σ_y is produced as a consequence of the flange stress equilibrium, because of the eccentricity e_f of the axial force N_f with respect to the web-flange junction. The resultant of stresses σ_y is null. The stress combination of σ_x, σ_y and τ_{xy}, can lead to the formation of cracks in the flange of a reinforced concrete T-beam [3]. The presence of transverse reinforcement or fibres in the concrete mass is necessary to guarantee the integrity of the section. This cracking adversely affects the service and ultimate performance of the beams. If the transverse reinforcement yields, a plastic redistribution of the tangential stresses along a beam zone can be assumed [1,2] (the tangential stress τ_{xy} distribution can be assumed uniform). Otherwise, if the transverse reinforcement does not yield, the web-flange tangential stress τ_{xy} should be calculated by elastic theory. In this case, the distribution of tangential stresses τ_{xy} is not uniform. In general, all codes coincide in attaching importance to guarantee the web-flange junction by a high enough minimum reinforcement ratio to have a tough ductile mechanism with either strut-and-tie model-based codes [1,2,4] or shear-friction model-based codes [5–9]. An adequate web-flange junction behaviour allows to take into account the contribution of the compressed flanges both for the flexural strength and for the vertical shear strength of beams with T-shaped sections. Although the present design codes ignore the contribution of flanges for shear strength, recent theoretical [10–13] and experimental studies [14–16] show that it is not negligible.”

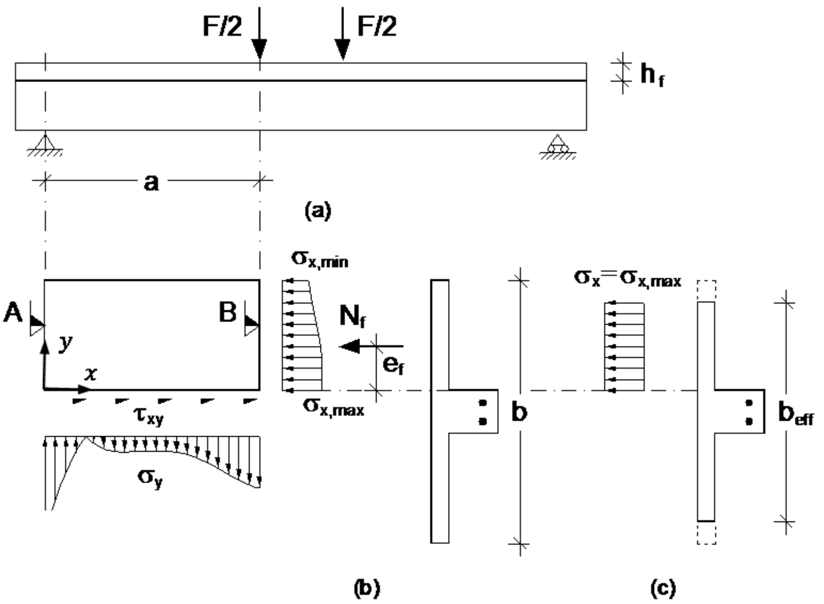

Figure 1: Flange stress distribution. (a) Test arrangement; (b) Actual flange stress distribution; (c) Flange effective width

1.1. On the evaluation of longitudinal shear in reinforced concrete members.

The beam model is imposed to evaluate longitudinal shear between the flange and web given its simplicity and wide acceptance. The flange effective width is needed to apply this model. It is a reduced flange width in which the normal stresses are supposed uniformly distributed in all flange points located at the same distance from the neutral fibre of the section (Figure 1.b and c). This uniform normal stress distribution replaces the actual non-uniform stress distribution that takes place as a result of the flexibility of the flanges in their plane. However, this phenomenon cannot be appreciated in T-beams with narrow flanges. As flange width increases, the normal stress is greater in the web-flange junction than in the end of the flange. The design codes [1,2,4,5] propose different expressions for the calculation of the flange effective width in the absence of a more precise determination (for example, FEM). The resultant of normal stresses in the effective flange width is calculated with the beam model and, based on this result, longitudinal shear is calculated along flange length. Other authors like Badawy and Bachmann [17] have proposed a global strut-and-tie model to study their five tested T-beams. The effective flange width is needed to apply this method as well.

Razaqpur and Ghali [3] applied a linear elastic analysis by finite elements to a variety of beams with different loading setups, with one span and two spans. They evaluated not only the longitudinal shear between the flange and web, but also the concomitant transverse axial load. The difference in the results between the beam model and the FEM model was not significant. Therefore, these authors concluded that more detail in evaluating longitudinal shear is not necessary, especially in beams with isostatic schemes. In addition, longitudinal shear is redistributed in the ultimate state [17–20].

The transverse axial load concomitant with the longitudinal shear between the flange and web is a force that the beam model is unable to provide, but can be evaluated with more complex models. Razaqpur and Ghali [3] and Páez and Díaz del Valle [21] used their elastic finite element model results to consider the concomitant transverse axial load to design flange transverse reinforcement. The problem is that using elastic results is not appropriate for proposing the design criteria of transverse reinforcement in the ultimate state. In this case, the plastic redistribution of internal forces is expected [18,20,22].

Morley and Rajendran [22] theoretically determined the effective width of beams by the so-called limit curves. This model was applied only to estimate the strength capacity of four beams previously tested by Davies [23]. These beams were made with not enough transverse reinforcement. Subsequently, Fiorito [19] and Tizatto [20] especially instrumented the flange to experimentally deduce the effective width value. Once the effective width is known, longitudinal shear can be more accurately assessed.

More sophistication can be applied to evaluate longitudinal shear by applying either finite elements with a non-linear analysis or the compression field theory. The advantage of these analyses is that they include the longitudinal shear evaluation and the response of the resistant mechanism in the same calculation. Hence they are able to provide the beam's strength capacity. Their disadvantages are their calculation cost and having to adjust many parameters.

1.2. On the longitudinal shear strength in reinforced concrete.

Longitudinal shear strength in T and I shape cross section RC beams is difficult to predict due to complex phenomena involved, such as the cracking induced anisotropy, the interaction with others forces as vertical shear or bending moment, the localization of the critical diagonal crack, the confinement effects of the flanges, the 3D flow of forces from the web to the flanges (shear lag effect), the interaction between concrete and reinforced or the size effect. The critical diagonal crack in T-beam has two branches. The first branch is more vertical and it is in the web. The second branch is more inclined and it is in the flange. The critical crack crosses the web, continues along the flange-web interface, until it propagates inclined inside the flange towards the load application point [24]. The crack inclination determines the strength capacity of the beam.

Several empirical and rational methods were developed taking as reference experimental results and theoretical studies to evaluate the longitudinal shear strength. Among these methods there is the Generalized Stress Field Approach (GSFA) [25–27], Modified Compressive Fields Theory (MCFT) [26], the strut-and-tie method (STM) [1,2,4], and the shear-friction method [5–9], as in a particular case of shear transference models.

Modified Compressive Fields Theory (MCFT) uses compatibility equations and non-linear constitutive laws for materials that consider the biaxial state of concrete strains. This rotating crack model provides accurate results compared with experimental tests. This method uses an iterative procedure to determine the inclination of the compressive struts. It can be employed for membrane elements subjected to in-plane normal and shear stresses, like the web and flanges of T-beam. Minelli and Vecchio

[28] validated MCFT-based numerical model with experimental results obtained on full-scale fibre-reinforced concrete (FRC). This numerical model adequately simulate the strength, stiffness, ductility, crack pattern development, and failure modes of all specimens tested. Other authors [29–31] applied MCFT-based numerical model to analyse the behaviour of elements made with steel fibres.

The strut-and-tie method allows analysing the beam behaviour as pinned statically determined strut-and-tie structure (Figure 2). The struts are the elements resistant to compression (concrete and compressed reinforcements), while the ties are the elements resistant to tension (tensioned reinforcements)." This method is used by European codes [1,2,4]. Badawy and Bachmann [17] resorted to the strut-and-tie method and tentatively proposed an angle of inclination of struts between 22º and 26.6º in compressed flanges. EC2 [2] includes the value of 26.6º as the minimum angle to be considered and EHE-08 [1] uses an angle of 45º by default, which doubles the required reinforcement. Tizatto and Shehata [32] recommended an angle that depends on flange dimensions.

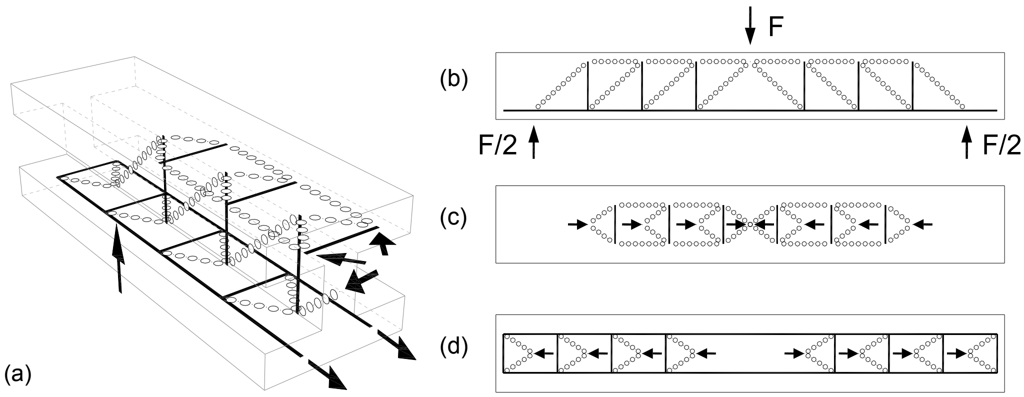

Figure 2: Strut-and-tie model of a pinned T-beam with a single load (a) 3D model; (b) Front view; (c) Flange top side plant view; (d) Flange bottom side plant view.

American standard ACI-318 [5] adopts the shear-friction model as a general method to study shear through a plane of weakness. Other American standards [6,7,9] and the Japanese JSCE/SSCS [8] adopt a linear model of friction plus cohesion (modified shear friction model).

1.3. On fibre-reinforced concrete (FRC).

There are experimental studies of reinforced concrete T-beams made of steel fibres [33–37]. These studies analyse the contribution of steel fibres in flexural strength or vertical shear. The relationship between the width and the thickness of the analysed T-beam flanges is moderate and, therefore, the flexibility of the flanges in their plane is reduced. In addition, these beams have been designed in order for the longitudinal shear not to be a failure mode. Consequently, no experimental results have been found for T-beams with wide flanges manufactured with FRC and tested to analyse the contribution of the fibres to the web-flange longitudinal shear resistance. Nevertheless, the vertical shear strength or the flexural strength of FRC has received plenty of attention and is included in design codes. Very few documents can be found on how to extend general models, such as strut-and-tie or shear-friction, to consider the effect of fibres on T-beams subjected to longitudinal web-flange shear. These models should consider the effectiveness of shear reinforcement mechanisms of fibres crossing the web-flange interface since it depends significantly on the fibre orientation. Fibres oriented with a certain angle to this interface do not provide any contribution. The fibre orientation and distribution is associated to the cast-in-place system.

The extension of the strut-and-tie method has received little attention in the scientific literature. There are some publications about simple structural elements, such as corbels [38–43], dapped-end beams [44–46], deep beams [47–50], bottle-shaped struts [51] or beams with span-depth ratio no more than 2.5 [52], which analyse how to include the effect of steel fibres. Fehling et al. [53] developed a proposal for the reduction of the compressive strength of cracked reinforced concrete. These authors considered the influence of fibres in addition to bar reinforcement. Campione [47] provided the only practical solution to determine strut compressive strength by considering the effect of steel fibres. Other studies have proposed using a term of residual tensile strength to be added to strength of reinforcement [54], as well as the possibility of using ties that derive exclusively from fibres [55]. López-Juárez, J A [56] describes more in detail strut-and-tie model applications to fibre reinforced concrete elements. Nothing was found about the shear friction model extension.

Empirical models [57–62] are the most widespread and contrasted, and are basically an image of the modified shear-friction models used in reinforced concrete, where fibres contribute as a term that is added to the reinforcement ratio. These empirical models are based on the results of push-off and prismatic tests.

After analysing the scientific literature, the objective of this research is to provide experimental results and to study the longitudinal shear between the flange and web in T-beams made with conventional concrete and FRC. The longitudinal shear of each tested beam and longitudinal shear cracking load were evaluated based on both a theoretical approach and the experimental results.

2. Experimental programme.

The objective of the experimental programme was to study 13 T-beams, of which four were made of conventional concrete and nine of FRC.

2.1. Test programme.

Thirteen isostatic 5-metre-long T-beams were tested. They were mounted onto two symmetric supports. The loading of these beams was applied at two symmetric points. Figure 3 depicts the loading configuration. Beams laid on two supports that allowed the rotation perpendicular to the bending plane. The horizontal movement was prevented in one of the supports, while the horizontal movement is allowed in the other end with the objective of avoiding the axial strain of the element. A steel beam was designed to divide the load of the actuator into two loading points, connected to a joint for keeping the load vertical all the time. This steel beam laid on two solid steel profiles placed on the beam. A neoprene layer was placed between the beam and each of the two solid steel profiles in order to regularize contact surface.

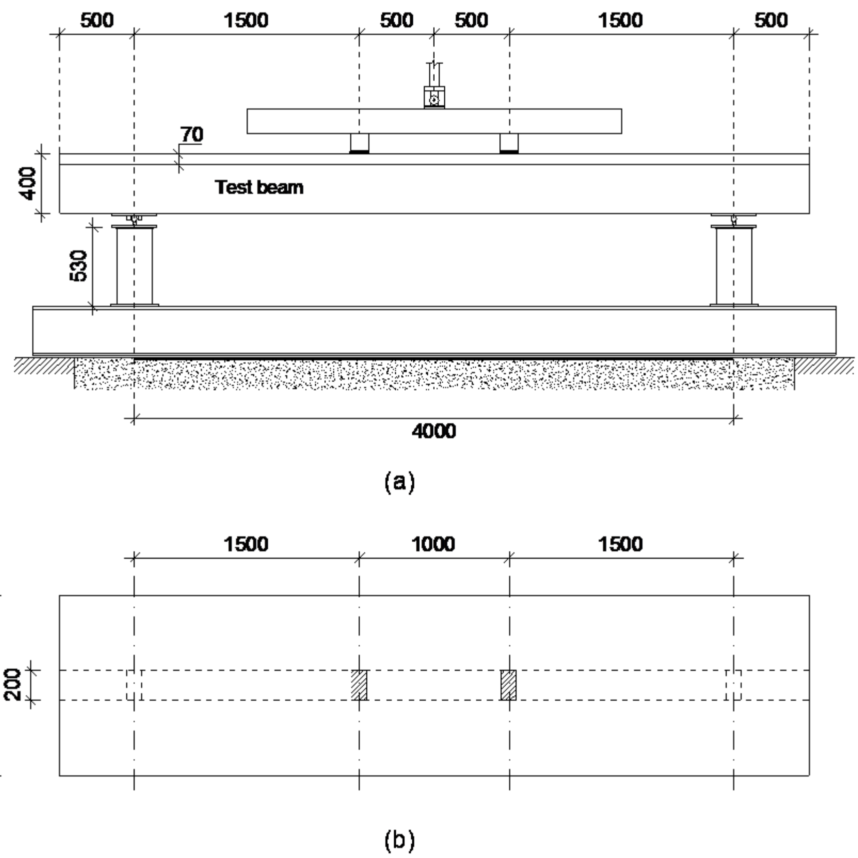

Figure 3: Loading configuration: (a) Front view, (b) Plan view. Units: mm.

The separation between loading points was slightly wider than twice the beam depth to ensure that the central section underwent the appropriate conditions to apply the classic beam theory hypotheses according to the Saint-Venant principle. Figure 6 shows the layout of a beam test.

Figure 4: Experimental test layout.

The cross section had flanges that were 1200 mm wide and 70 mm thick. Flange size is similar than the one used by other authors [17–20,63]. A flange size (width and thickness) was considered with the objective of studying longitudinal shear behaviour at web-flange junction (strength and failure mode). Flange size was defined so as the vertical load that causes web-flange junction cracking by longitudinal shear was half the vertical load that theoretically causes bending failure. The total cross section depth was 400 mm with a web thickness of 200 mm (Figure 5). The distribution of the longitudinal and transverse reinforcements in the web was the same in all specimens. Initially, geometrical concrete cover r (Figure 5.b) was established at 30 mm, but was modified during the experimental campaign (Table 1) to change the longitudinal shear failure plane. Figure 5 displays the cross section geometry and the longitudinal reinforcement arrangement. A longitudinal reinforcement ratio was arranged in order for the entire flange to be compressed in ultimate state. In this way, the maximum web-flange longitudinal shear was obtained. Table 1 shows the depth values at which the longitudinal reinforcements were located in each specimen.

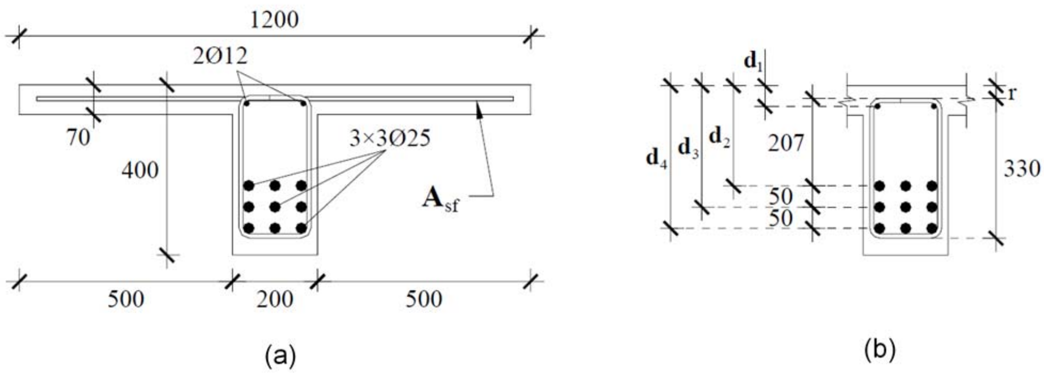

Figure 5: Cross section: (a) Geometry and longitudinal reinforcement arrangement; (b) Longitudinal reinforcement locations. Units: mm.

r	d_1	d_2	d_3	d_4	Specimens
30	49	247	297	347	V1-0, V2-0
25	44	242	292	342	V3-0, V4-0, V2-20, V3-20, V1-40
12	31	229	279	329	V1-20, V1-30, V2-30, V3-30, V2-40, V3-40

Table 1: Geometric concrete cover and reinforcement depths (units: mm)

The web transverse reinforcements consisted of either single or double Ø10 stirrups, with the distribution indicated in Figure 6. The transverse reinforcement ratio is conditioned by the longitudinal reinforcement required ratio to obtain the maximum web-flange longitudinal shear. Transverse reinforcement is provided in the web so that the theoretical load of the beam that causes vertical shear failure is much greater than the load that causes bending failure. A holder was provided at the ends of specimens to lift them.

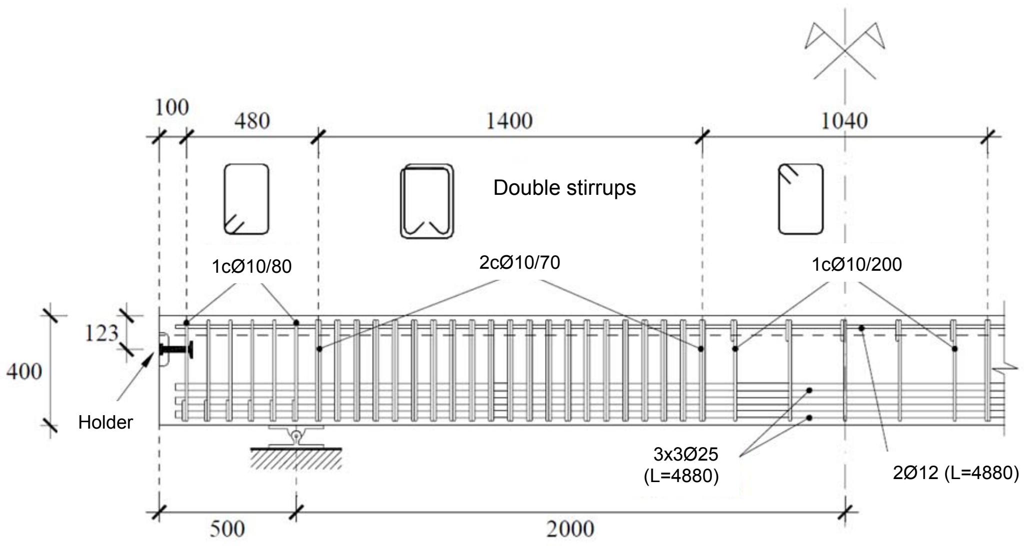

Figure 6: Web's transverse reinforcements. Units: mm.

The study parameters of the experimental programme were the transverse reinforcement ratio in flanges and the steel fibre content. The beams were manufactured with an insufficient theoretical transverse reinforcement ratio to force the web-flange longitudinal shear failure and thus analyse the contribution of the fibres. The EC2 [2] was applied to determine the minimum required transverse reinforcement in the flanges, by choosing the maximum possible plastic redistribution length and the lowest strut inclination angle according to EC-2 [2] . According to section 6.2.4 (3) of EC2 [2], the maximum value of the plastic length that can be considered is half the distance between the zero bending moment and the maximum bending moment (750 mm). This value cannot be greater than the distance between loading points. If a greater plastic redistribution length was chosen, the mean web-flange longitudinal shear would be smaller. In the absence of more rigorous studies, section 6.2.4 (4) of EC2 [2] provides a range for the strut inclination angle (θ_f) in the compressed flanges: 1 ≤ cot θ_f ≤ 2. If cot θ_f = 2 (θ_f = 26.5º) is adopted, the minimum value for the flange transverse reinforcement is obtained. The theoretical ultimate moment of the T-beam cross section was calculated according to the EC2 [2] for plain concrete beams. This moment was determined by adopting the parabola-rectangle law for concrete, the elasto-plastic law for reinforcement and the classic hypothesis of sectional analysis: (1) plane sections remain plane; (2) the strain in the bonded reinforcement is the same as that in the surrounding concrete; (3) limit strains are defined by EC2 [2] for the ultimate limit state: reinforcing steel tension strain limit $\varepsilon_{ud} = 10‰$ taken from EHE-08 [1]; concrete compression strain limit $\varepsilon_{cu2} = 3.5‰$ concrete pure compression strain limit $\varepsilon_{c2} = 2.0‰$. The flange effective width according to EC2 [2] was considered to calculate the ultimate bending moment. The flange effective width coincides with the actual width of 1200 mm for the T-beam cross section geometry and the distance between points of zero moment of 4000 mm. A minimum amount of 568 mm²/m was determined for the transverse reinforcement ratio. The following four amounts of transverse reinforcement (A_{sf} in Figure 5.a) were established based on the minimum amount: 87.5 mm²/m (7Ø8 in 4 m), 179.5 mm²/m (Ø8/280 mm), 359 mm²/m (Ø8/140 mm) and 561 mm²/m (Ø10/140 mm). These amounts represent 15.5, 31.6, 63.2 and 98.8% of the minimum reinforcement amount. No beam with zero transverse reinforcement was analysed as there was a minimum of 7Ø8 bars, which would be used to stick on strain gauges to measure flange transverse strains. The minimum fibre content was established as the minimum for the concrete to be considered FRC for structural purposes. The minimum content was 20 kg/m³ according to EHE-08 [1] and approximately matched the 0.3% of CNR-DT 204 [31]. A maximum steel fibre content of the 40 kg/m³ was established by manufacturer's recommendations, and an intermediate value corresponding to 30 kg/m³ was also chosen. According to the recommendations of the Model Code 2010 [4], a FRC was designed for a toughness class 1.5d.

Table 2 shows the details of the 13 specimens. The difference between them lay in the steel fibre content (4 made with conventional concrete and 9 with FRC) and in the flange transversal reinforcement area (A_{sf}). Four families of beams were established. The steel fibre content varied within each family, except for specimen V4-0, which consisted of a single reinforced concrete beam that was adopted as a reference beam.

Family	Flange transverse reinforcement area (A_{sf})	Steel fibre content kg/m³			
		0	20	30	40
V1	87.5 mm²/m [7Ø8 in 4 m]	V1-0	V1-20	V1-30	V1-40
V2	179,5 mm²/m [Ø8/280mm]	V2-0	V2-20	V2-30	V2-40
V3	359,0 mm²/m [Ø8/140mm]	V3-0	V3-20	V3-30	V3-40
V4	561,0 mm²/m [Ø10/140mm]	V4-0	-	-	-

Table 2: Specimen notation.

Figure 7 displays the distribution of the flange transverse reinforcements. This distribution corresponded to the assembly indicated in Table 2. The web-flange longitudinal shear is theoretically zero in the central part of the beam, between the loading points. Nevertheless, a quantity of flange transverse reinforcement slightly lower than that at the beam ends was arranged.

2.2. Material characterisation.

A nominal compressive concrete strength of 25 MPa was set. This strength is representative of most buildings and construction members. Dose consisted of 1100 kg/m^3 of sand 0/4, 880 kg/m^3 of gravel 6/12, 300 kg/m^3 of cement 42.5R, 1.8 l/m^3 of superplasticiser additive ACE 425 of BASF and 150 l/m^3 of water. As mentioned above, the steel fibre contents were 0, 20, 30 and 40 kg/m³. The type of steel fibres was BASF Masterfiber 530, whose yield stress was higher than 3000 MPa, 30 mm long, 0.35 mm in diameter, with a slenderness of 86 and an elastic modulus of 190 GPa.

Concrete compressive strength was obtained by testing three cylindrical 150×300 mm test pieces of each specimen according to UNE-EN 12390-3:2009 [64]. The average value ($\bar{\sigma}$) and coefficient of variation (CV) of the concrete compressive strength are shown in Table 3, where f_{cm} is the mean compressive strength. The time from manufacturing to testing is also depicted in Table 3 (concrete age in days). These values were lower than expected because the concrete mixer had a minimum volume of 1.5 m³ to guarantee correct mixing, but only 1 m³, corresponding to each beam, was used.

Apart from the cylindrical specimens, three prismatic specimens, measuring 150×150×580 mm, were obtained from each concrete mixture to test flexural tensile strength according to UNE-EN 14651 [65]. The average value ($\bar{\sigma}$) and coefficient of variation (CV) of the flexural tensile strength are shown in Table 3, where f_{LOP} is the limit of proportionality in the flexural tensile strength test and $f_{R,j}$ (for j =1–4) corresponds to crack mouth opening displacements (CMOD) of 0.5, 1.5, 2.5 and 3.5 mm, respectively. The distance between the bottom of the specimen and the displacement transducer used to measure the CMOD was 6 mm. This value was slightly higher than the maximum value recommended by UNE-EN 14651 [65]. To correct the error, the proposal of Ferreira et al. [66] valid for distances between 0 and 10 mm was employed. These authors proposed correction factors that depended on the relative height of the crack. A more detailed description can be found in [56] about the used correction and the obtained results (load-CMOD diagrams).

Specimen	Age (days)	f_{cm} (MPa)		f_{LOP} (MPa)		$f_{R,1}$ (MPa)		$f_{R,2}$ (MPa)		$f_{R,3}$ (MPa)		$f_{R,4}$ (MPa)	
		$\bar{\sigma}$ (MPa)	CV (%)	$\bar{\sigma}$ (MPa)	CV (%)	$\bar{\sigma}$ (MPa)	CV (%)	$\bar{\sigma}$ (MPa)	CV (%)	$\bar{\sigma}$ (MPa)	CV (%)	$\bar{\sigma}$ (MPa)	CV (%)
V1-0	29	19.7	2.0	3.3	6.5	-	-	-	-	-	-	-	v
V2-0	28	20.7	9.1	3.1	8.0	-	-	-	-	-	-	-	
V3-0	28	20.6	14.8	3.1	3.2	-	-	-	-	-	-	-	
V4-0	27	20.2	2.8	3.1	3.8	-	-	-	-	-	-	-	
V1-20	36	19.0	9.2	3.1	6.5	1.0	20.0	1.1	23.6	1.1	18.4	1.1	18.4
V2-20	28	19.9	1.0	3.1	1.6	1.0	32.9	1.1	31.0	1.1	31.0	1.1	36.4
V3-20	33	21.0	11.7	3.5	1.6	1.0	10.0	1.1	5.4	1.1	5.4	1.1	5.4
V1-30	30	23.6	9.2	3.5	4.7	1.9	14.9	2.1	14.8	2.2	12.0	2.1	9.5
V2-30	29	20.5	1.7	3.3	0.0	1.9	30.0	2.0	33.1	2.0	33.1	1.9	31.6
V3-30	34	22.4	4.2	2.9	6.1	1.5	4.9	1.6	9.4	1.6	13.7	1.5	18.9
V1-40	39	21.2	3.4	3.3	2.9	2.1	20.1	2.4	20.8	2.5	20.0	2.4	18.2
V2-40	41	22.0	5.1	3.5	8.8	2.8	11.0	2.9	8.8	2.8	7.3	2.8	5.5
V3-40	40	19.0	8.5	3.2	6.5	2.5	11.3	2.9	9.8	2.8	12.4	2.7	10.5

Table 3: Mechanical properties of concrete.

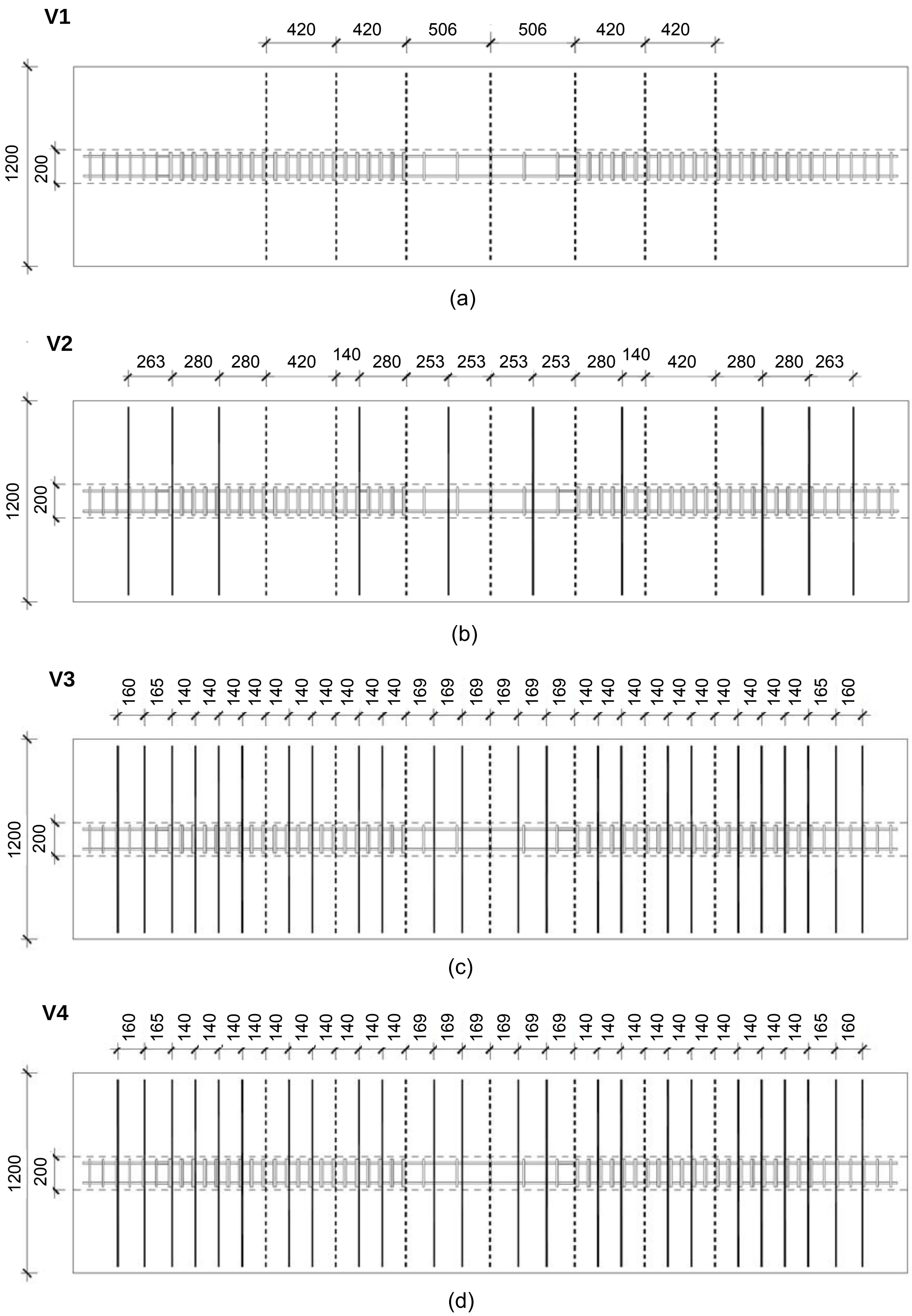

Figure 7: Flange transverse reinforcement arrangement: (a) Family V1; (b) Family V2; (c) Family V3; (d) Family V4. Units: mm.

The steel used in all the beam reinforcements was B500SD. Three bar samples were selected from each diameter before being tested according to the procedure established in UNE-EN 10002-1 [67]. The average value ($\bar{\sigma}$) and coefficient of variation (CV) of the mechanical properties of reinforcements are shown in Table 4. In this table, f_y, ε_y, f_{sh}, ε_{sh}, f_u, ε_u, E_s are respectively the yield stress, the strain that corresponded to the yield stress, the stress at which the hardening branch began, the strain associated with f_{sh}, the maximum stress, the strain associated with the maximum stress and the elasticity modulus.

The beams were horizontally in inverted position and on an externally-vibrated form.

	Longitudinal				Transverse			
	Ø12		Ø25		Ø8		Ø10	
	$\bar{\sigma}$ (MPa)	CV (%)	$\bar{\sigma}$ (MPa)	CV (%)	$\bar{\sigma}$ (MPa)	CV (%)	$\bar{\sigma}$ (MPa)	CV (%)
f_y (MPa)	552	1.3	552	1.1	592	1.4	531	1.2
ε_y	0.0026	3.8	0.0028	3.7	0.0027	3.6	0.0026	4.0
ε_{sh}	0.0300	3.2	0.0235	4.1	0.0200	2.3	0.0375	5.3
f_u (MPa)	658	0.6	660	0.7	662	0.7	638	0.7
ε_u	0.1220	2.7	0.1041	3.1	0.0412	0.1	0.1671	5.2
E_s (MPa)	209685	4.1	195414	5.3	223320	7.0	206180	4.2

Table 4: Mechanical properties of reinforcements.

2.3. Instrumentation.

The vertical load was applied by the hydraulic actuator and was controlled by a 1000kN load cell. A LVDT was arranged in the central section of each specimen to measure vertical displacement (LVDT-1, see Figure 8). Six strain gauges were arranged in the central section of the specimens: two on the longitudinal steel reinforcements (channel 2 and 3, Figure 8) located on the most tensioned and most compressed bars of the section, and four of them were placed on concrete in the longitudinal direction of the beam, across the flanges (channel 5-8, Figure 8). In addition, seven strain gauges were arranged on the transverse reinforcements located on the flanges at the web-flange junction (channel 9-15, Figure 9).

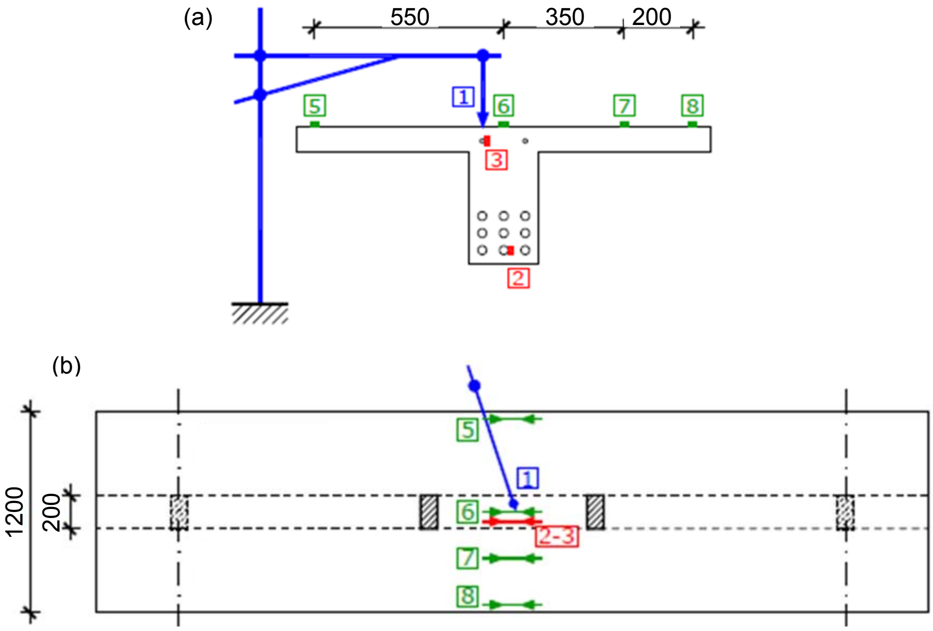

Figure 8: LVDT to measure displacement at midspan, strain gauges on concrete top side and strain gauges on longitudinal reinforcements. (a) Front view, (b) Plan view. Units: mm.

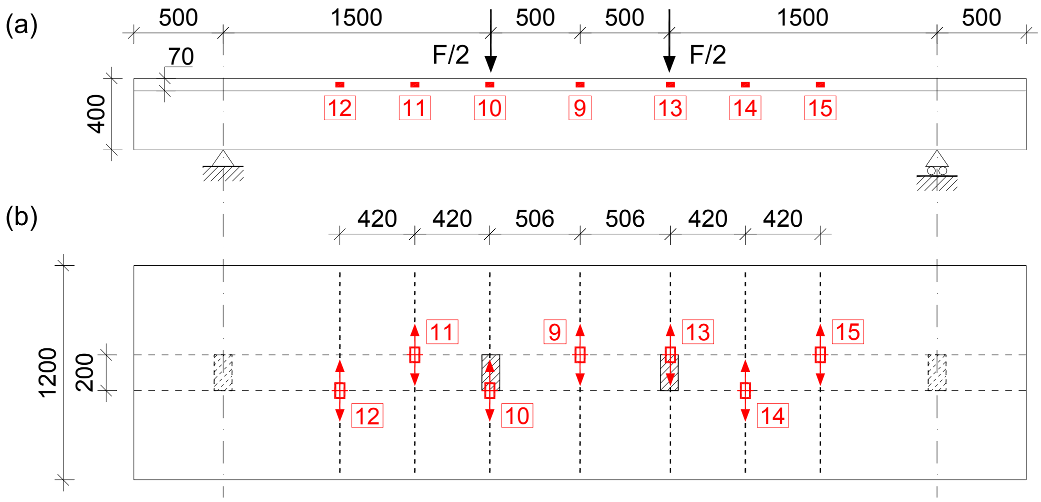

Figure 9: Strain gauges on flange transverse reinforcements: (a) Front view, (b) Plan view. Units: mm.

Web-flange junction is subjected to both tangential stresses (τ_{xy}) and transverse axial stresses (σ_y), see Figure 1.b. These stresses act simultaneously with the longitudinal sectional forces (bending moment and vertical shear). According to Razaqpur and Ghali [3], the transverse axial stress (σ_y) in the flange is compressive in the vicinity of the supports, at a distance of less than 10% of span length, for the loading scheme of tests. This compressive axial stress is resisted by concrete [3]. According to these authors [3], the transverse axial stress in the flange (σ_y) is tensile in the rest of the span, and is maximum under the loading point. Consequently, the strain gauges numbered from 9 to 15 (see Figure 9) were arranged along the beam in the transverse reinforcements, without covering the length around the supports. This was achieved by using 7Ø8 in all the beams, except in reference beam V4-0 which had 7Ø10.

3. Experimental results.

The experimental results corresponding to the 13 tested T-beams are described in this section.

3.1. Strength capacity and failure modes.

Table 5 summarises the main results. It shows the maximum load F_u and the maximum experimental bending moment in central section $M_{E,max}$ of all the tested specimens. As expected, the higher the transverse reinforcement ratio, the greater the strength capacity of the beams. In general, a higher steel fibre content in the concrete mass improved the strength capacity of beams, except for the VN-40 type beams. This was due to possible errors while manufacturing beams, perhaps because the concrete mixture was not homogeneous.

3.2. Strain plane of the central section.

Table 5 includes the midspan longitudinal bar strains called ε_{s2} for the most tensioned bars (from channel 2 in Figure 8), and ε_{s3} for the most compressed bars (from channel 3 in Figure 8) for the maximum load situation. Table 5 also includes the strain on the most compressed edge of section ε_{c6} (from channel 6 in Figure 8) and the depth of neutral fibre x calculated from strains ε_{s2} and ε_{s3}. It was not possible to determine depth x in four beams (V2-20, V3-20, V2-30 and V3-30) as gauges failed before reaching the maximum load. As seen, depth x was greater than flange thickness (70 mm) in all cases and, consequently, the entire flange was compressed. In addition, the most tensioned reinforcements were yielded in six of the 13 beams (strain greater than 2.8 ‰). The most tensioned reinforcements came close to the yield in the other beams.

Beam	F_u (kN)	$M_{E,max}$ (kNm)	ε_{s2}[*] (‰)	ε_{s3}[*] (‰)	ε_{c6}[*] (‰)	x (mm)	Failure mode
V1-0	375.0	281.2	-1.986	1.385	0.828	171.4	Web-flange shear V
V2-0	506.2	379.7	-3.552	2.215	2.918	163.5	Web-flange shear H
V3-0	533.0	399.7	-2.857	1.223	1.826	133.3	Web-flange shear H
V4-0	536.2	402.2	-4.235	1.453	2.293	120.1	Vertical shear H
V1-20	455.9	341.9	-2.533	2.378	1.605	175.3	Web-flange shear V
V2-20	589.1	441.8	-1.240 [**] (M_E=194.9)	3.848	1.871	-	Web-flange shear H
V3-20	691.2	518.4	-6.372 [**] (M_E=480.6)	5.736 [**] (M_E=515.4)	2.919	-	Bending with longitudinal shear cracking
V1-30	546.9	410.2	-5.120	3.565	2.841	153.3	Web-flange shear V
V2-30	634.6	475.9	-3.636	2.201 [**] (M_E=428.4)	2.322	-	Bending
V3-30	663.5	497.6	-4.493	1.611 [**] (M_E=465.0)	[*]	-	Bending with longitudinal shear cracking
V1-40	494.9	371.1	-2.421	1.084	1.440	136.2	Vertical shear H
V2-40	530.9	398.2	-2.749	1.520	1.671	137.1	Bending
V3-40	496.3	372.2	-2.671	1.446	1.844	135.7	Bending

[*] Compression strain positive.
[**] Failure of strain gauges. The last recorded value for the moment M_E is displayed.

Table 5: General results in the ultimate state.

3.3. Failure modes.

Table 5 shows the five failure types identified in this experimental programme: the longitudinal shear between the flange and web according to the vertical plane of the web-flange junction (Web-flange shear V in Table 5) (Figure 10.a-b); longitudinal shear according to a horizontal surface tangent to stirrups (Web-flange shear H in Table 5) (Figure 10.a-c); bending with concrete crushing and the local buckling of the compressed reinforcements (Bending in Table 5) (Figure 10.d-f); bending with concrete crushing with an advanced state of longitudinal cracking due to the shear between the flange and web (Bending with longitudinal shear cracking in Table 5) (Figure 10.g-h); shear in the web because of concrete crushing due to the presence of hollows in concrete (Vertical shear H in Table 5) (Figure 10.i).

In general, longitudinal cracking occurred at the web-flange junctions. This cracking first appeared on the bottom edge of the encounter. Diagonal cracking was also produced with an inclination angle of 45º in relation to the beam's longitudinal axis (Figure 10.h). Cracking formation followed a double transversal and longitudinal symmetry pattern, but failure was not symmetrical. Only one of the four possible flange parts separated from the core.

The web-flange longitudinal shear failure occurred in 6 out of 13 beams. The failure plane was vertical in three specimens (V1-0, V1-20 and V1-30) according to the vertical plane (1-2) in Figure 10.a and b. The failure plane was horizontal in the other 3 specimens (V2-0, V3-0 and V2-20) according to the horizontal plane (1-3) in Figure 10.a and c. The horizontal failure plane occurred in the first beams that were tested, because the employed geometrical concrete cover was excessive in comparison with the flange thickness (25/30 mm vs 70 mm). When using 30 mm separators on the stirrups, the web transverse reinforcement remained in the lower half of the flange thickness, which was 70 mm. The legs of the transverse reinforcement of the web introduced an abnormal failure plane, disturbing significantly the development of the other failure mechanism. The concrete cover was reduced to 12 mm, which resulted in two more web-flange longitudinal shear failures (V1-20 and V1-30) according to a vertical surface type 1-2 (Figure 10.a). By reducing the coating, web-flange longitudinal shear in plane 1-3 decreased.

Three beams failed due to the longitudinal shear between the flange and web according to the vertical plane of the web-flange junction (web-flange shear V in Table 5). This failure mode was observed in beams V1-0, V1-20 and V1-30, which had the lowest flange transverse reinforcement ratio (15.5% of the minimum transverse reinforcement ratio) and had a steel fibre content lower or equal to 30 kg/m^3. In ultimate situation, the flange longitudinal and inclined cracking were very visible and the relative displacement between the flange and the web was important (Figure 10.b). The separation between the flange and the web took place in beam V1-0, which has no steel fibres, and some transverse bars broke. The insufficient fibre content together with a very small flange transverse reinforcement ratio resulted in the loss of integrity of the section.

The failure mode due to a longitudinal shear according to horizontal surface tangent to stirrups (Web-flange shear H in Table 5) occurred in three specimens: beams V2-0 and V3-0, which had a geometrical concrete cover of 25 or 30 mm, a flange transverse reinforcement ratio lower than required (31.6% and 63.2%) and no steel fibres and in beam V2-0 with a 31.6% of the required transverse reinforcement ratio and with a low fibre content (20 kg/m^3). In these cases, a relative web-flange displacement was observed. The entire flange separated from the web in the case of beam V2-0 with no steel fibres (Figure 10.c). The insufficient combination of the flange transverse reinforcement and the steel fibres content in addition to the excessive geometrical concrete cover meant the integrity loss of the cross section.

The bending failure mode (Bending in Table 5) occurred in three specimens: V2-40, V3-40 and V2-30. The beams V2-40 and V3-40 had higher fibre content (40 kg/m^3) and a transverse reinforcement ratio in the flanges lower than required (31.6% and 63.2%). The beam V2-30 had 31.6% of the required transverse reinforcement ratio and 30 kg/m^3 of fibre content. The longitudinal and inclined cracking network in the flanges was difficult to observe. In these specimens, a combination of fibre content (greater than or equal to 30 kg/m^3) and a flange transverse reinforcement ratio were sufficient to control the crack width and ensure the integrity of the section. In general, the failure mode was brittle due to concrete crushing in the loading section (Figure 10.d). The tensioned longitudinal reinforcement remained in the elastic range, except in beam V2-30. In addition, the compressed reinforcement buckled when the concrete cover spalled (Figure 10.e and f).

Two beams underwent bending failure with longitudinal shear cracking (Bending with longitudinal shear cracking in Table 5). This failure occurred in beams V3-20 and V3-30, which had 60% of the required flange transverse reinforcement ratio and a fibre content of 20 kg/m^3 and 30 kg/m^3. This failure corresponded to an intermediate situation between bending failure and web-flange longitudinal shear failure. In this case, the longitudinal and inclined cracking network in the flanges was visible (Figure 10.g). The combination of transverse reinforcement with the steel fibres was sufficient to control the crack width and the integrity of the section. There was not any relative web-flange displacement either. The failure was due to concrete crushing in the loading section (Figure 10.g), with longitudinal reinforcement yielding and with a significant web-flange longitudinal shear cracking (Figure 10.h).

Finally, an unexpected failure by vertical shear occurred in beams V1-40 and V4-0 due to the presence of the hollows in the web. The cause of these hollows was a poor concrete compaction (Vertical shear H in Table 5). The presence of hollows reduced both the strength capacity of the struts and the adherence of the longitudinal reinforcements. This combined effect can be observed in the web in Figure 10.i.

In short, the longitudinal shear between flanges and web failure took place in the beams with less transverse reinforcement (V1-0, V1-20 and V1-30), except in beam V1-40. This exception was due to lack of concrete compaction and the consequent vertical shear failure. The bending failure mode went from longitudinal shear to bending in two situations: (1) in the specimens with a 31.6% transverse reinforcement ratio of the required one and a fibre content of 30 kg/m^3 or higher; (2) in the specimens with a 63.2% transverse reinforcement ratio of the required one and a minimum fibre content of 20 kg/m^3. The proper combination of transverse reinforcement and fibre content in these beams was sufficient to control the longitudinal cracking in the web-flange junction and ensure the integrity of the section. In these beams, there was a failure mode by concrete crushing (Figure 10.d and g), with or without visible web-flange junction cracking. The incorporation of steel fibres into concrete not only increased strength capacity, but also modified the failure mode, from web-flange longitudinal shear to bending.

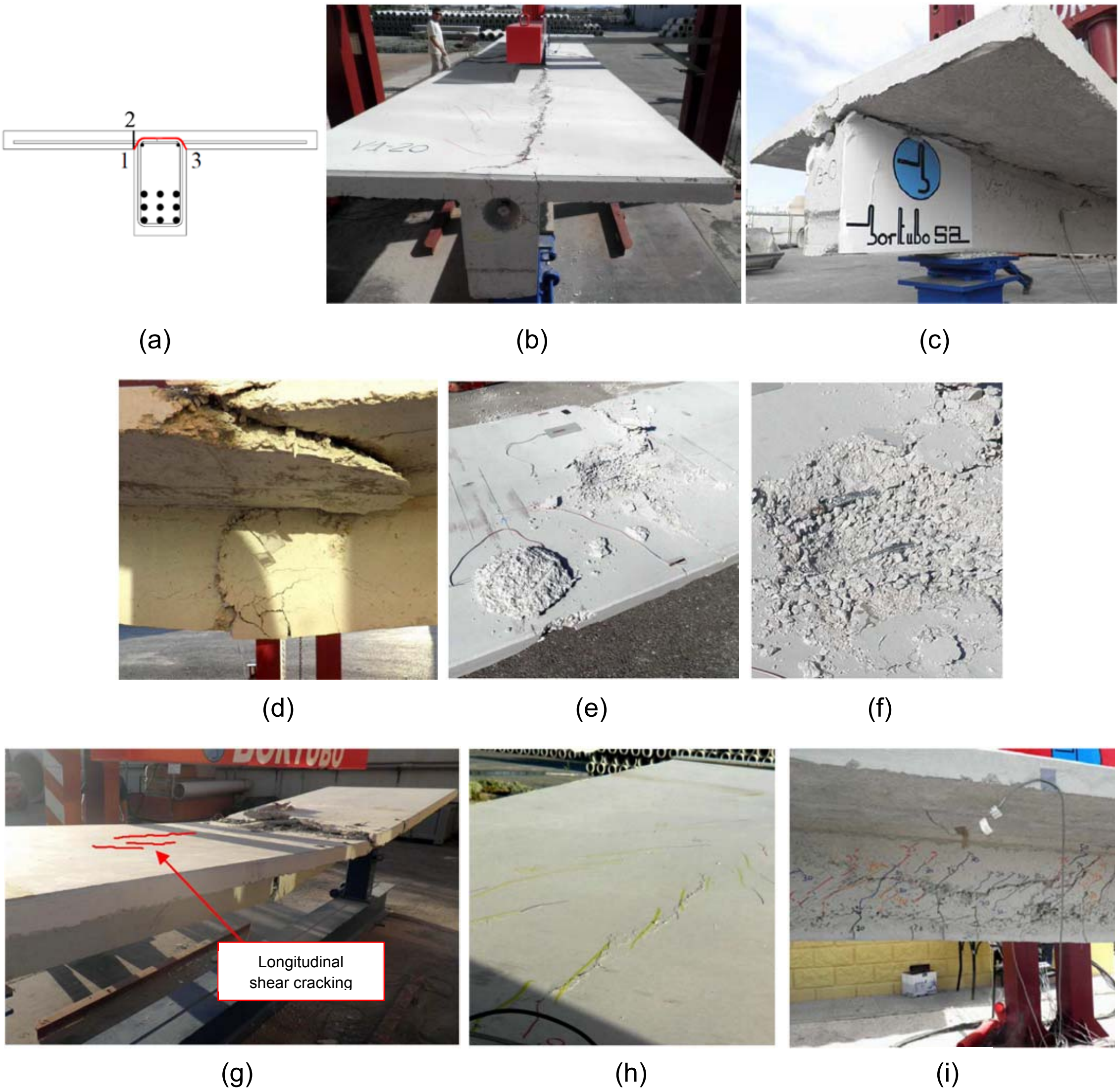

Figure 10: Specimen failure modes: (a) Possible web-flange longitudinal shear failure planes: 1-2 vertical plane, 1-3 horizontal plane; (b) Web-flange longitudinal shear H (V3-0); (c) Web-flange longitudinal shear V (V1-20); (d) Bending failure (V2-30): web and flange bottom part view; (e) Bending failure (V2-30): flange top side view (concrete crushing); (f) Bending failure (V2-30): compressed reinforcement buckling detail; (g) Bending with longitudinal shear cracking (V3-20), general post-test specimen view; (h) Bending with longitudinal shear cracking (V3-20), detail of shear cracks on the flange top side; (i) Vertical shear H, due to the presence of hollows in concrete (V1-40).

3.4. Flange longitudinal strains.

Flange compressive longitudinal strains (ε_{ci}, where i is the number of the channel) could only be measured at four points (channel 5-8, Figure 8). This information was useful in order to verify if the whole flange width was effective to validate the classic sectional analysis. According to the formulation of EC2 [2], the theoretical effective width coincided exactly with the actual width. However, the tested beams had the particularity of possessing a deficient transverse reinforcement area to bear longitudinal shear, which can be partially compensated with steel fibres.

Figure 11 represents the flange longitudinal strain profile for different load levels (F_j) across flanges. The recorded values are only displayed until the beam's maximum load. The two cases in Figure 11 reflect the general behaviour of the 13 tested beams. A reduction in the effective width value was observed as the load level increased in the beams with either a smaller transverse reinforcement area or a lower steel fibre content. However, codes like EC2 [68] affirm that effective width is the same in both the service limit and ultimate limit states, as explained by Hendy and Smith [69]. This is no contradiction as the explanation lies in the deficient transverse reinforcement area. In general, a decrease in effective width began when longitudinal web-flange cracking appeared, just as the increase in the strain at the web-flange junction showed (Figure 11). In general, the family of VN-40 beams were the least affected, as were the beams with the biggest transverse reinforcement area of each family.

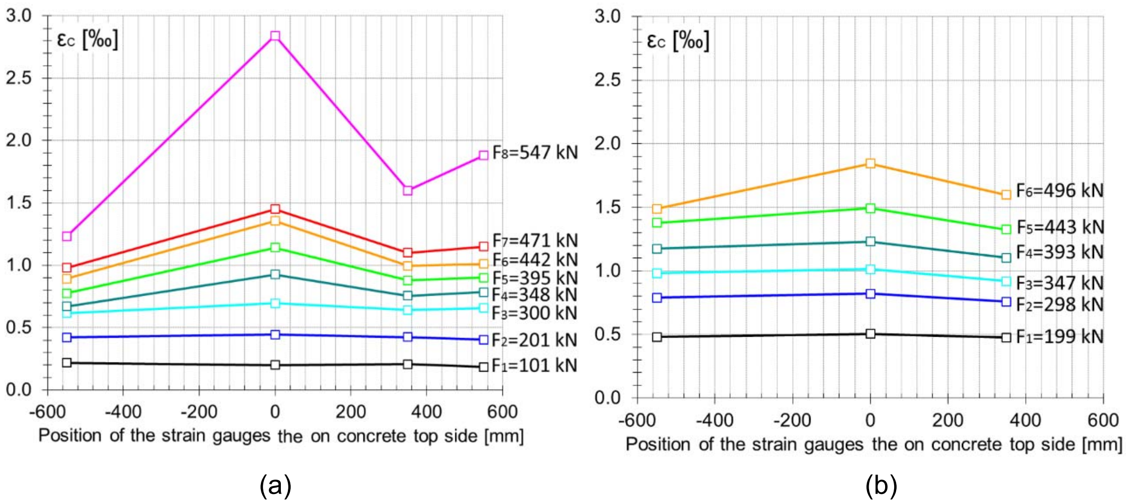

Figure 11: Longitudinal strains across the flange: (a) Web-flange longitudinal shear V failure (beam V1-30), (b) Bending failure (beam V3-40). [Compressive strain ε_c (> 0)].

3.5. Flange transverse strains.

Flange transverse strains were measured thanks to the arrangement of the seven strain gauges in the transverse reinforcements (channel 9-15, Figure 9). Figure *12* represents the strain evolution of each gauge in relation to the total load applied to the beam, where ε_{si} is the strain recorded by the strain gauge corresponding to channel-i (see Figure 9). Two beams are shown as representative examples of flange-web longitudinal shear failure according to a vertical plane and bending failures: beams V1-20 (Figure 12.a) and V3-40 (Figure 12.b), respectively. The leaps that are seen in the strains are due to the load increase was stopped to observe the cracking. The first zone of load – flange transverse strain diagram is lineal in both cases. A jump was perceived in most of the gauges of beam V1-20 at around a load value of 300 kN (Figure 12.a), while this was perceived for only one gauge in beam V3-40 and to a lesser extent (Figure 12.b). The jump was followed by a higher growth rate in the strain value. This jump could only be justified by the increase in the transverse reinforcement tension level when cracking took place, which was more marked in those flanges with either a smaller transverse reinforcement area or fewer steel fibre content. Figure 12 shows how in beam V1-20, which has a smaller amount of transversal reinforcement and fibre content, undergoes a greater strain increase than beam V3-40, which has a higher amount of transversal reinforcement and fibre content.

Figure 12.a also shows how the gauge recordings of the V1-20 transverse reinforcements shot up at values close to the maximum load. This was due to transverse reinforcement yielding. Gauges ε_{s10} , ε_{s14} and ε_{s15} failed before the maximum load was reached. Figure 12.b displays how the transverse reinforcement of specimen V1-30 did not yield because the higher recorded strain was 2.5‰, which was less than the yield strain (2.7‰). Figure 13 shows the state of one of the flange transverse reinforcements of beam V1-0.

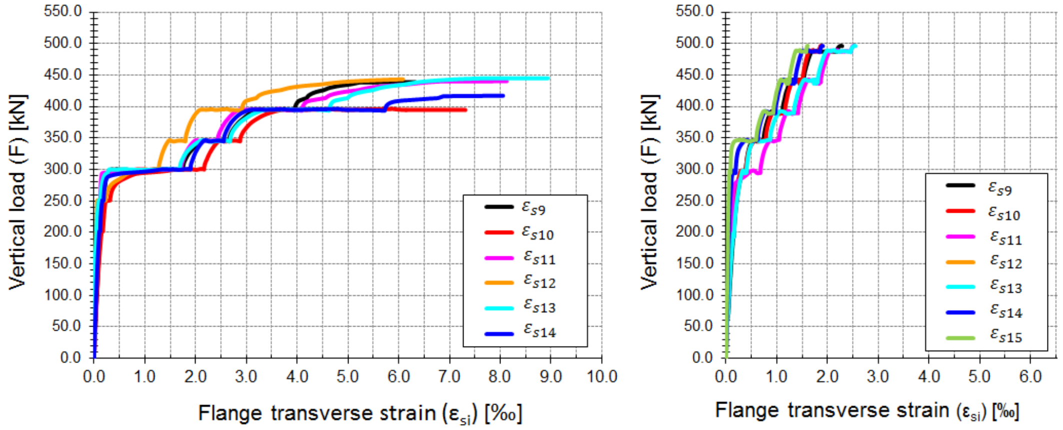

(a) (b)

Figure 12: Vertical load – flange transverse strain diagrams: (a) Beam V1-20 (web-flange longitudinal shear V failure); (b) Beam V3-40 (bending failure). [Tensile strain ε_{si} (>0)].

(a) (b)

Figure 13: Final appearance of a flange transverse reinforcement, beam V1-0: (a) The remaining longest part of a reinforcement that broke, approximately 200 mm over the web plus 450 mm corresponding to the flange at one-side; (b) Detail of the strain gauge location zone.

3.6. Vertical load – displacement.

Figure 14 shows three vertical load - midspan displacement diagrams corresponding to three beams with different failure modes, which are representative of the other beams. More detailed information of the experimental results can be found in [56].

These diagrams have a first initial region with a more marked slope (Figure 14.a, slope I), which corresponds to the uncracked elastic state, followed by another region that was almost rectilinear with a less pronounced slope, which corresponded to the cracked elastic state (Figure 14.a, slope II). The completion of this second rectilinear region occurred when one of the failure modes started, as noted in Table 5. In all cases, the failure mode is brittle, since there is no plastic deformation before reaching the ultimate load.

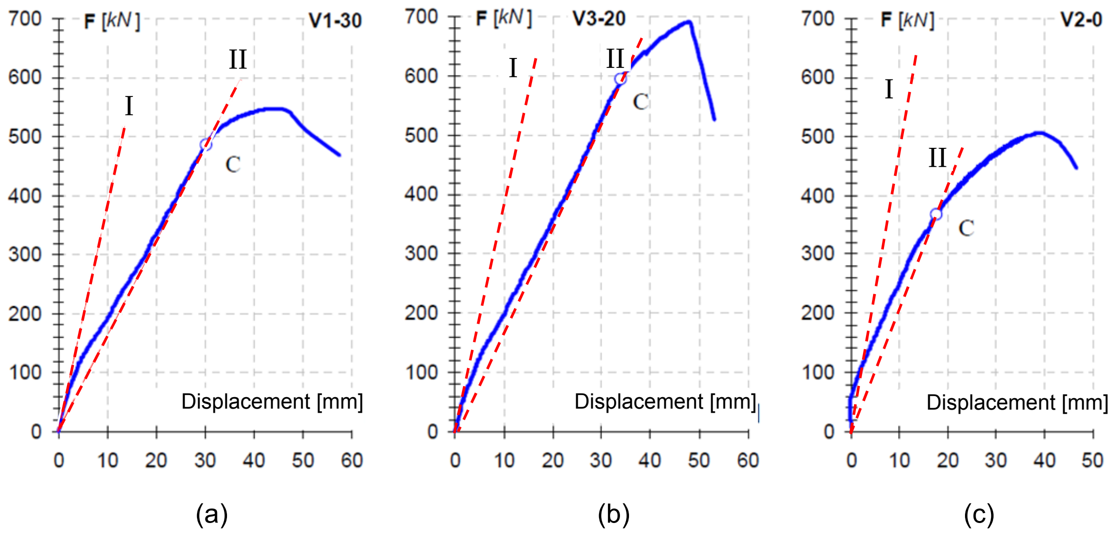

Figure 14: Vertical load-displacement in the midspan diagrams: (a) Specimen V1-30, the web-flange longitudinal shear failure according to a vertical plane; (b) Specimen V3-20, bending failure with longitudinal shear cracking; (c) Specimen V2-0, web-flange longitudinal shear failure according to a horizontal plane.

Point C is indicated in Figure 14 and corresponds to loss of linearity. Point C is identified with two phenomena for beam V1-30 (Figure 14.a), which failed by longitudinal shear between the flange and web along a vertical plane: the beginning of the tensile longitudinal reinforcement yielding and the beginning of the flange transverse reinforcement yield. Point C is identified with tensile longitudinal reinforcement yielding in beam V3-20 (Figure 14.b), which failed by bending with concrete crushing, while the flange transverse reinforcement strains continued to grow (no sudden growth was recorded, as in the previous case). Finally, point C corresponds to a sudden strain jump of more than 1‰ in four of the seven strain gauges located at the flange reinforcements in beam V2-0 (Figure 14.c), which failed by longitudinal shear between flanges and the web along a horizontal plane. In this case, the most tensioned longitudinal reinforcements were not yielded.

4. Analysis of the experimental results.

Both the web-flange longitudinal shear cracking vertical load and the mean web-flange longitudinal shear in the maximum load situation are determined in this section

4.1. Web-flange longitudinal shear cracking vertical load.

In order to theoretically calculate the cracking vertical load ($F_{f,crack}$) corresponding to longitudinal shear of the web-flange junction, flange effective width was determined with the equations of the following codes: EC2 [2], EHE-08 [1] and EH-91[70], based on the Brendel [71] proposal (Table 6). The EC2 [2] equation, which coincides with CM 2010 [4], provides the highest value. The effective width b_{eff} proposed by the EC2 [2] (1200 mm) for the determination of the vertical load $F_{f,crack}$ has been adopted for the following reasons: (1) According to Hendy and Smith [72], the value of the effective width proposed by the EC-2 [2] approximates the elastic values; (2) The distribution of the longitudinal strain across the flange is uniform for loads lower than the vertical load of experimental cracking $F_{f,crack}$ (Figure 11). No equation contemplated the dependence of the effective width with the flange transverse reinforcement ratio.

Effective width b_{eff}(mm)	All limit states
EC2 [2] and CM 2010 [4]	1200
EHE-08 [1]	1000
EH-91 [70] (Brendel [71])	880

Table 6: Flange effective width according to several codes and authors.

Longitudinal shear cracking occurred for a vertical load value that came close to 300 kN in all the experimental tests. This load was determined from a jump in the strains recorded by the gauges located in the flange transverse reinforcements and also visually (Section 3.5).

The cracking vertical load $F_{f,crack}$ of the web-flange junction is assessed in a similar way to Regan and Placas [18] and Tizatto [20]. Unlike these authors, the formulation proposed by Razaqpur and Ghali [3] was used to calculate the transverse axial force N_y and the variation of the normal stresses was considered according to the flange thickness. The approach to the problem is illustrated in Figure 15. The problem was simplified by symmetry (Figure 15.a). The ABCD flange region was delimited (Figure 15.b). The membrane stresses applied to the flange are represented (Figure 15.c-e), based on the applied load.

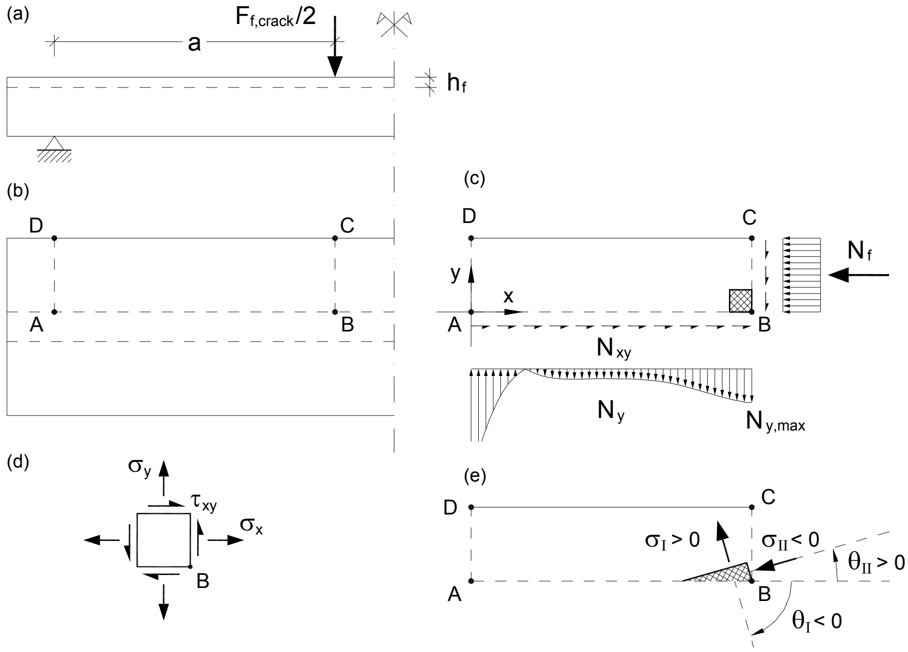

Figure 15: Scheme to determinate the web-flange longitudinal shear cracking vertical load ($F_{f,crack}$): (a) Frontal view; (b) Plan view; (c) Flange stresses on ABCD; (d) Stresses on B; (e) Principal stresses on B.

Point B, located under the load application point, was the point at which the maximum transverse tensile force per unit length $N_{y,max}$ was produced together with a maximum value for N_f. The sign criterion for stresses is schematised in Figure 15.d. The principal directions are illustrated in Figure 15.e, where σ_I and σ_{II} are the principal tensile and compressive stresses, respectively.

The criterion for evaluating load $F_{f,crack}$ was to establish the principal tensile stress at point B (Figure 15) that equalled the mean concrete tensile strength (f_{ctm}):

$$\sigma_I = f_{ctm} \tag{1}$$

The principal tensile stress (σ_I) at point B is calculated from the following expression

$$\sigma_I = \frac{\sigma_x + \sigma_y}{2} + \sqrt{\left(\frac{\sigma_x - \sigma_y}{2}\right)^2 + \tau_{xy}^2} \tag{2}$$

where:

σ_x $= -|N_f|/(b_{eff} \cdot h_f)$, longitudinal stress in the flange plane in x direction

σ_y $= |N_{y,max}|/h_f$, transverse stress in the flange plane in y direction

τ_{xy} $= -|N_{xy}|/h_f$, tangential stress in the flange plane

h_f: Flange thickness

b_{eff}: Effective width of flange

N_f: Axial force in the flange

$N_{y,max}$: Maximum transverse tensile force per unit length

N_{xy}: Longitudinal shear load per unit length

There are no direct data available on tensile strength f_{ctm}. Therefore, the mean value of tensile strength was estimated from the compressive strength f_c according to Section 5.1.5.1. of Model Code 2010 [4] (see Table 7).

	$f_c\ (MPa)$	$f_{LOP}\ (MPa)$	$f_{ctm}\ (MPa)$	$M_{b,crack}\ (kNm)$	$F_{b,crack}\ (kN)$
V1-0	19.7	3.3	2.11	40.3	53.8
V2-0	20.7	3.1	1.98	37.6	50.2
V3-0	20.6	3.1	1.98	36.9	49.2
V4-0	20.2	3.1	1.98	37.0	49.4
V1-20	19.0	3.1	1.98	35.6	47.4
V2-20	19.9	3.1	1.98	37.1	49.4
V3-20	21.0	3.5	2.23	41.6	55.4
V1-30	23.0	3.5	2.23	39.3	52.4
V2-30	20.5	3.3	2.11	37.2	49.6
V3-30	22.4	2.9	1.85	32.6	43.4
V1-40	21.2	3.3	2.11	39.2	52.2
V2-40	22.0	3.5	2.23	39.5	52.6
V3-40	19.0	3.2	2.04	36.7	49.0

Table 7: The mean concrete tensile strength (f_{ctm}), cracking bending moment ($M_{b,crack}$) and the load ($F_{b,crack}$) that caused the cracking bending moment.

Table 7 also shows both the bending moment ($\mathrm{M_{b,crack}}$) and load ($\mathrm{F_{b,crack}}$) of each beam which produced bending cracking. The own-weight bending moment (6.562 kNm), and the flexural tensile strength f_{LOP} determined in the prismatic specimens tests were considered to calculate the cracking bending moment. The mechanical characteristics of the homogenised section and the maximum effective width provided by the regulations (Table 6) were used to calculate them. Beam V3-20 presented the highest cracking moment $M_{b,crack}$ (41.6 kNm), which corresponded to a load $F_{b,crack}$ of approximately 55.5 kN (Table 7). This value was much lower than the load that led the longitudinal cracks to appear at the web-flange junction observed in the tests, which was around 300 kN for all the specimens (Section 3.5). Therefore, when longitudinal cracks appeared at the vertical web-flange junctions, bending cracks previously appeared. Hence membrane stresses must be determined using the sectional parameters by assuming that the section is cracked.

The axial force in flange N_f can be obtained approximately with Equation (3), which arises from integrating the sectional stresses at point B (Figure 15):

$$N_f \cong \frac{S_{f,crack}}{I_{crack}}\left(F_{f,crack}/2 \cdot a + M_g\right) \quad (3)$$

where:

$S_{f,crack}$: Static moment of the flange in the cracked state in relation to the cracked cross section's centre of gravity in plain concrete

I_{crack}: The cross section's inertia moment in the cracked state in relation to the cracked cross section's centre of gravity in plain concrete

a: Length between the support and loading point (Figure 15.a).

M_g: Bending moment due to own weight in the load applying section (M_g= 6.562 kNm).

The contribution of the fibres has been neglected for the calculation of the mechanical characteristics of the section, $S_{f,crack}$ and I_{crack}, due to the important amount of longitudinal reinforcement arranged in the section. This approach allows both calculating the mechanical characteristics of the section independently of the applied sectional forces and simplifying the expressions to determine the forces in the flange plane (N_f, N_y and N_{xy}).

Longitudinal shear load per unit length N_{xy} was assessed at point B (Figure 15) with the following equation:

$$N_{xy} \cong \frac{S_{f,crack}}{I_{crack}}\left(F_{f,crack}/2 + V_g\right) \quad (4)$$

where:

V_g: Vertical shear due to own weight in the load applying section (V_g=1.875 kN).

The formulation of Razaqpur and Ghali [3] was used to determine the transverse tensile force per unit length $N_{y,max}$ at point B (Figure 15), which is the stress that the classic beam model is unable to provide. The result, considering own weight, gave this equation (5):

$$N_{y,max} \cong \frac{S_{f,crack}}{I_{crack}}\left[(b-b_w)\cdot 0.4\cdot q+\frac{(F_{f,crack}/2)}{4}\right] \quad (5)$$

where: $\mathrm{b} = 1.2$ m, $\mathrm{b_w} = 0.2$ m, $\mathrm{q} = 3.75$ kN/m.

Point B in Figure 15 underwent the maximum value of σ_I by considering how the membrane stresses were distributed according to line AB of the flange, and by observing the equation of principal tensile stress σ_I (1). Tensile stress σ_y (>0) decreased rapidly from point B to point A. The magnitude of compression σ_x (<0) also displayed the same behaviour, but more smoothly. Web-flange tangential stress τ_{xy} remained constant because vertical shear remained constant before the onset of cracking at point B. Thus, the principal tensile stress descended from point B to point A. When the study point moved from B toward the midspan, tensile stress σ_y remained constant, and practically the same happened with compressive stress σ_x as the effect of own weight was minimal. On the contrary, tangential stress τ_{xy} became null theoretically. For this reason, the principal tensile stress value was also lower in the central region of the beam between loading points.

The stresses formulated in (1) - (2) represent average values along flange thickness at point B (Figure 15). To contemplate the fact that longitudinal compressive stress σ_x could considerably vary along thickness, two more options were added to the determination of the web-flange longitudinal cracking load. They consisted in formulating the normal stresses on the top ($\sigma_{x,top}$) and bottom ($\sigma_{x,bot}$) flange sides. For the longitudinal stresses at point B, the equations below were used:

$$\sigma_{x,top} \cong -\frac{F_{f,crack} \cdot a + M_g}{I_{crack}} x_{crack} \quad (6)$$

$$\sigma_{x,bot} \cong -\frac{F_{f,crack} \cdot a + M_g}{I_{crack}} (x_{crack} - h_f) \quad (7)$$

where x_{crack} is the depth of the cracked section's centre of gravity, measured from the top side; and M_g = 6.562 kNm is the bending moment due to own weight.

For transverse stresses σ_y at point B, which tend to be less important than longitudinal stresses, the variation caused by transverse bending due to the flange's own weight was considered in the top ($\sigma_{y,top}$) and bottom ($\sigma_{y,bot}$) flange sides, and resulted in:

$$\sigma_{y,top} \cong \sigma_y + 0.27 \text{ (MPa)} \quad (8)$$

$$\sigma_{y,bot} \cong \sigma_y - 0.27 \text{ (MPa)} \quad (9)$$

where σ_y is the transverse tensile stress, equal to $|N_{y,max}|/h_f$.

Figure 16 shows the web-flange longitudinal shear cracking vertical load ($F_{f,crack}$). That is, the load that satisfied Equation (1) calculated with average stresses, top side stresses and bottom side stresses at point B. The cracking vertical load $F_{f,crack}$ needed to cause the principal stress to reach the concrete tensile strength value was lower when the condition was applied to the flange bottom side, which indicates that longitudinal cracking started on the bottom side to finally propagate through the thickness toward the top side.

Table 8 shows the detailed results for the bottom side stresses condition at point B. An effective width of the flange b_{eff} = 1200 mm was considered to obtain the results shown in Figure 16 and Table 8. As further data of interest, the main compression stress σ_{II}, whose equation was analogous to (2), is included in the tables, but with a minus sign accompanying the root term. The principal directions, as illustrated in Figure 15, were defined with the following equations:

$$\theta_{II} = \frac{1}{2} \cdot arct\left(\frac{2\tau_{xy}}{\sigma_x - \sigma_y}\right) \quad (10)$$

$$\theta_I = \theta_{II} - 90° \quad (11)$$

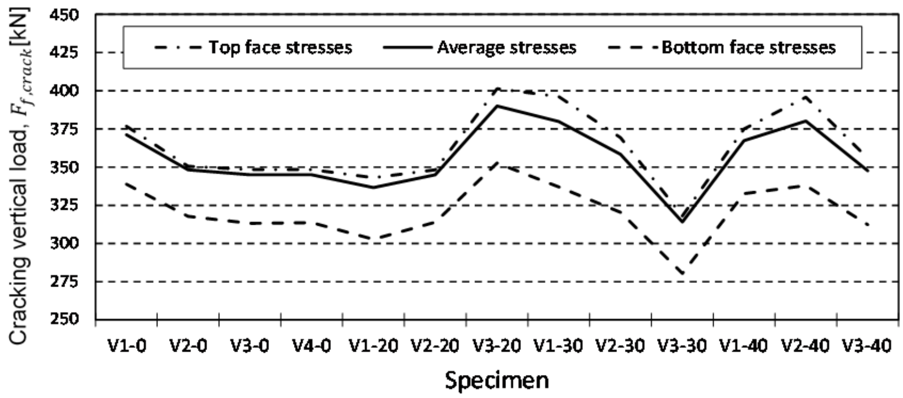

Figure 16: The vertical load $F_{f,crack}$ that caused web-flange cracking.

Beam	$F_{f,crack}$ (kN)	N_f (kN)	N_{xy} (kN)	$N_{y,max}$ (kN)	$\sigma_{x,bot}$ (MPa)	τ_{xy} (MPa)	$\sigma_{y,bot}$ (MPa)	$\sigma_{I,bot}$ (MPa)	$\sigma_{II,bot}$ (MPa)	$\theta_{I,bot}$ (º)	$\theta_{II,bot}$ (º)
V1-0	338.80	378.10	248.40	65.40	-6.64	-3.55	0.66	2.11	-8.08	-67.90	22.10
V2-0	317.70	355.50	233.30	61.50	-6.14	-3.33	0.61	1.98	-7.51	-67.70	22.30
V3-0	313.20	356.60	234.00	60.70	-6.11	-3.34	0.60	1.98	-7.49	-67.60	22.40
V4-0	313.60	356.80	234.20	60.70	-6.13	-3.35	0.60	1.98	-7.51	-67.60	22.40
V1-20	302.70	360.00	236.10	58.70	-6.10	-3.37	0.57	1.98	-7.51	-67.30	22.70
V2-20	313.90	357.00	234.30	60.80	-6.14	-3.35	0.60	1.98	-7.52	-67.60	22.40
V3-20	352.60	400.20	263.10	68.00	-6.99	-3.76	0.70	2.23	-8.53	-67.80	22.20
V1-30	337.00	400.90	263.40	65.10	-6.77	-3.76	0.66	2.23	-8.34	-67.30	22.70
V2-30	320.40	380.90	250.10	62.00	-6.46	-3.57	0.62	2.11	-7.95	-67.40	22.60
V3-30	280.40	335.30	219.60	54.50	-5.49	-3.14	0.51	1.85	-6.83	-66.90	23.10
V1-40	332.60	378.10	248.40	64.30	-6.54	-3.55	0.65	2.11	-7.99	-67.70	22.30
V2-40	337.90	401.80	264.00	65.30	-6.82	-3.77	0.66	2.23	-8.39	-67.40	22.60
V3-40	312.30	371.10	243.60	60.50	-6.32	-3.48	0.59	2.04	-7.77	-67.40	22.60

Table 8: Web-flange longitudinal shear cracking vertical load. Stress condition applied to the low flange side at point B: $\sigma_{I,inf}$=f_{ctm} for effective width b_{eff}=1200 mm.

The average analytical force $F_{f,crack}$ value that produced longitudinal cracking was 321.00 kN, with a standard deviation of 14.16 kN, for the case of effective width b_{eff} = 1200 mm and by assuming that cracking started on the bottom side. The variations in the values between specimens were due to the differences in both the values of the concrete tensile strength and the effective depth which modified the sectional parameters. The average force $F_{f,crack}$ value that produced longitudinal cracking, in accordance with the experimental results (Section 3.5), was approximately 300 kN. Consequently, when comparing the theoretical and experimental force $F_{f,crack}$ values that produced longitudinal cracking, effective width b_{eff} = 1200 mm was suitable for the service state before longitudinal web-flange cracking took place. This behaviour was also observed in the tests performed by Tizatto [20]. The analytical process shown in this section also corroborated that onset of cracking occurred on the bottom side, which coincides with the experimental observations made by other authors [32].

The methodology proposed in this section to calculate the vertical cracking load $F_{f,crack}$ can be applied to determine a minimum flange transverse reinforcement ratio that avoids a brittle flange failure. For this purpose, the amount of transverse reinforcement needed to resist the load $F_{f,crack}$ will be determined e.g. using a strut-and-tie model or a shear friction model. A minimum flange transverse reinforcement ratio is required if the load $F_{f,crack}$ is lower than the theoretical load that would produce beam failure because of either bending or vertical shear.

4.2. The mean web-flange longitudinal shear assessment.

This section shows the procedure to obtain the mean web-flange longitudinal shear stress during the loading process until failure based on the experimental results.

4.2.1. Analytical approach.

An analytical approach is proposed to evaluate the mean longitudinal shear stress τ_{xy} at the web-flange junction in a region 1.5-metre length [1,2] (from the support to the loading point, see Figure 3). This mean stress τ_{xy} is $\Delta F_f/(h_f \cdot \Delta x)$, where ΔF_f is the change of the normal (longitudinal) force in the flange in this region, h_f is the flange thickness and Δx is the length under consideration equal to 1.5 metre. According to the loading scheme of the specimens (Figure 3), only one of these sections (over support or under the loading point) was studied due to symmetry. The supporting section presented a null bending moment and the section under the loading point presented a maximum bending moment if own weight was neglected. Thus, the force ΔF_f is equal to compressive axial load in the flange N_f at the section under the loading point.

The compressive resultant force N_f, which was determined by integrating compressive stresses into the flange, was calculated in the maximum bending moment section for each load level. It was firstly necessary to transform the moment – curvature diagram (M–χ) into a moment – flange compressive load (M–N_f).

Curvatures were obtained from the data provided by the strain gauges located in both the longitudinal reinforcements (ε_{s2} and ε_{s3}) (Figure 8) and the most compressed side of concrete (ε_{c6}) at the midspan section (Figure 8). Thus the strain plane of the section could be determined at each load level if experimental curvature χ_E and experimental bending moment M_E were known because axial force was zero. To do this, a system of two non-linear equations, which corresponded to the two equilibrium equations of the section (Equations (12) - (13)), was solved. The unknowns of the system were the strain at the reference centre of sectional forces ε_0 and the effective section width b_{eff} (Figure 17).

$$N_t(\varepsilon_0; b_{eff}) = 0 \tag{12}$$

$$M_t(\varepsilon_0; b_{eff}) = M_E \tag{13}$$

where:

N_t: The resultant axial force determined by integrating the normal stresses of the section.

M_t: The resultant bending moment determined by integrating the normal stresses of the section.

Therefore, internal stresses (N_t and M_t) were determined by integrating sectional stresses based on both the strain plane of the section (ε_0 and χ_E) and the constitutive equations of the materials, which relate stresses with strains. The constitutive equations selected for concrete and steel are indicated below.

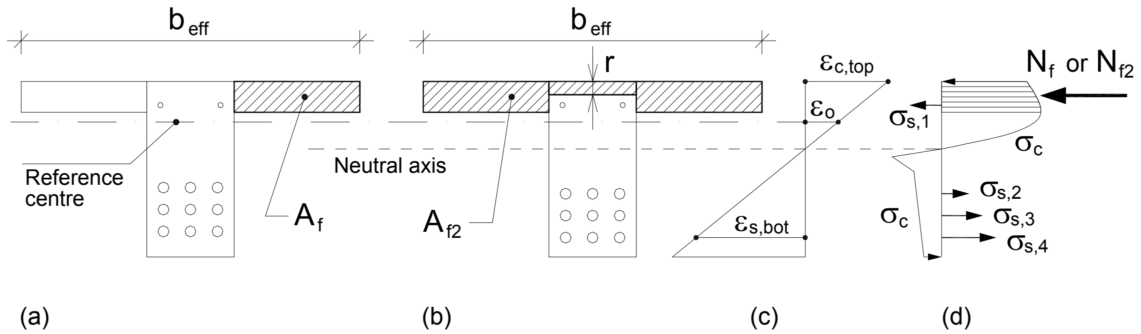

Figure 17: Compressive axial load in the flange: (a) Web-flange longitudinal shear failure according to a vertical plane; (b) Web-flange longitudinal shear failure according to a horizontal plane (specimens V2-0, V3-0 and V2-20); (c) Generic strain plane of the section; (d) Generic stress diagram of a section.

4.2.2. Material constitutive models.

The constitutive equation proposed by Campione [73] (Equation (14)) was used for modelling concrete behaviour under compression (Figure 18.a). The input data of Campione's expression are fibre factor F_V and concrete compressive strength without considering steel fibres f_c. In the present study, however, the compressive strength of the concrete with fibres f_{cf} was known. Therefore, this compressive strength was used directly. This law is also useful for non-FRC by simply imposing $F_v = 0$.

$$\sigma_c(\varepsilon_c) = f_{cf} \cdot \frac{\left(\frac{\varepsilon_c}{\varepsilon_{f0}}\right) \cdot \beta}{\beta - 1 + \left(\frac{\varepsilon_c}{\varepsilon_{f0}}\right)^{\beta}} \tag{14}$$

where:

f_{cf}: Maximum compressive stress of the σ–ε curve.

$$f_{cf} = f_c + 6.913 \cdot F_V \ [MPa]$$

ε_{f0}: Strain corresponding to f_{cf}.

$$\varepsilon_{f0} = 0.0016 + 0.00002 \cdot f_{cf} + 0.00178 \cdot F_V \ [MPa]$$

β: $$\beta = \begin{cases} 1.4276 \cdot e^{0.0247 \cdot (f_{cf} - 6.913 \cdot F_V)} & \text{for} \quad 0 \le \varepsilon \le \varepsilon_{f0} \\ 1.4276 \cdot e^{0.0247 \cdot (f_{cf} - 6.913 \cdot F_V)} + 0.175 \cdot F_V & \text{for} \quad \varepsilon_{f0} < \varepsilon < \varepsilon_{cu} \end{cases} \ [MPa]$$

F_V: Fibre factor.

$$F_V = V_f \left(\frac{L_f}{D_f}\right)$$

V_f: Ratio between steel fibre volume and concrete volume.

L_f: Steel fibre length.

D_f: Steel fibre diameter.

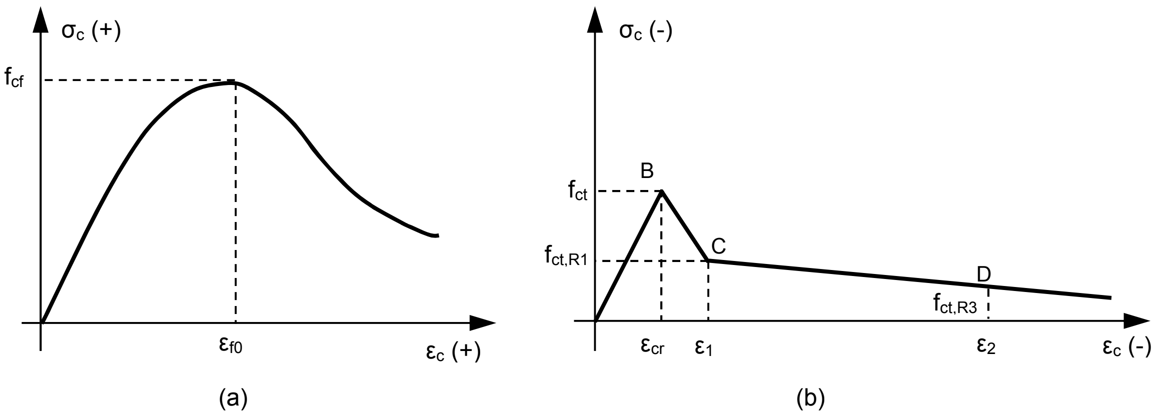

Figure 18: Complete concrete constitutive law: (a) Behaviour under compression (Campione [73], positive compression); (b) Behaviour under tension (EHE-08 [1], negative tension).

Regarding tension behaviour, the trilinear constitutive law for concrete under tension proposed by EHE-08 [1] (Equation (15)) (Figure 18.b) was used.

$$
\begin{array}{llll}
\text{Point B:} & f_{ct} = 0.6 \cdot f_{LOP} & \text{for} & \varepsilon_{cr} = 1000 \cdot \frac{f_{Ft}}{E_{co}} \\
\text{Point C:} & f_{ct,R1} = 0.45 \cdot f_{R,1} & \text{for} & \varepsilon_1 = \varepsilon_{cr} + 0.1‰ \\
\text{Point D:} & f_{ct,R3} = k_1 \cdot \left(0.5 f_{R,3} - 0.2 f_{R,1}\right) & \text{for} & \varepsilon_2 = \frac{2.5}{l_{cs}}
\end{array}
\qquad (15)
$$

where ε_{cr}, ε_1 and ε_2 are expressed as per thousand [‰]; E_{c0} is the concrete elasticity modulus; $k_1 = 1$ for bending; and l_{cs} is the critical length in metres ($l_{cs} = min(s_m,\ h - x)$), where s_m is the average separation between cracks, h is the height of the T-beams and x is the depth of the neutral axis. According to EHE-08 [1] for SFRC with softening behaviour and with $f_{R3} < 3$ MPa (Table 3), the separation s_m can be calculated without considering the steel fibre contribution (as plain concrete). The separation s_m was less than $(h - x)$ in all specimens, therefore the critical length l_{cs} was equal to s_m. Critical length l_{cs} was 141 mm for beams V1-20, V1-30, V2-30, V3-30, V2-40, V3-40 and was 115 mm for beams V2-20, V3-20, V1-40.

The constitutive law for reinforcements is elastoplastic. Elasticity modulus E_s and yield stress f_y are the same as those shown Table 4.

4.2.3. Determination of the compressive resultant load in flange $\mathbf{N_f}$.

In the general case, the specimens' cross section can be divided into three rectangles, as indicated in Figure 17.a. However, there were three specimens whose failure occurred by longitudinal shear according to a horizontal plane formed over web stirrups: V2-0, V3-0 and V2-20. In this case, the cross section was simplified into four rectangles, as shown in Figure 17.b. For these three specimens, the resultant compressive load on flange N_{f2} was obtained from the two rectangles of width b_{eff} that constituted the flange on each side of the core, plus the central rectangle with a height that equalled geometric concrete cover r. The fourth rectangle formed the rest of the web: 200 mm wide and 400-r height.

The process to determine the resultant compressive load on the flange according to a vertical failure plane (N_f, see Figure 17.a), and the resultant compressive load on the flange according to a horizontal failure plane (N_{f2}, see Figure 17.b), consisted of dividing the section into the elements indicated in Figure 17 and following these steps:

(1) An initial value was established for effective width: b_{eff} = 1200 mm if the procedure began. Otherwise the effective width took the value of the previous iteration.

(2) From the axial force equilibrium (Equation (12)), the value of the strain at the reference centre of sectional forces ε_0 was obtained as the experimental curvature for each load level was known.

(3) After obtaining ε_0, the bending moment equilibrium was stated (Equation (13)) to determine effective width b_{eff}. For this purpose, bending moment M_t was compared with experimental moment M_E. If $|M_{tot} - M_E| \leq 0.001\ \mathrm{kNm}$, then a satisfactory solution was found and step (4) was followed. If $M_t - M_E > +0.001\ \mathrm{kNm}$, a lower value was adopted for b_{eff} and step (2) was repeated. If $M_t - M_E < -0.001\ \mathrm{kNm}$, a higher value was adopted for b_{eff} and step (2) was repeated.

(4) Finally, when ε_0 and b_{eff} were obtained, the axial compressive force of flange N_f was determined. The mean longitudinal shear stress at the web-flange junction τ_{xy} was obtained as the quotient between the force N_f and the failure surface along the considered beam region.

(5) Go back to step (1) until the maximum moment in the section under the loading point.

The analytical model was validated based on experimental results. Figure 22 compares the experimental bending moment M_E with both then strain at the reference centre of sectional forces ε_0 obtained experimentally and ε_0 obtained analytically. The experimentally obtained strain ε_0 was computed from strain gauges located in both the longitudinal reinforcements (ε_{s2} and ε_{s3}) (Figure 8) and the most compressed concrete side (ε_{c6}) at the midspan section (Figure 8). The analytical values of ε_0 are computed according to equations (15) and (16). The experimental moment (M_E) – strain (ε_0) diagram is represented in this figure. A sufficient approximation between the experimental results and the analytical model is observed in this figure.

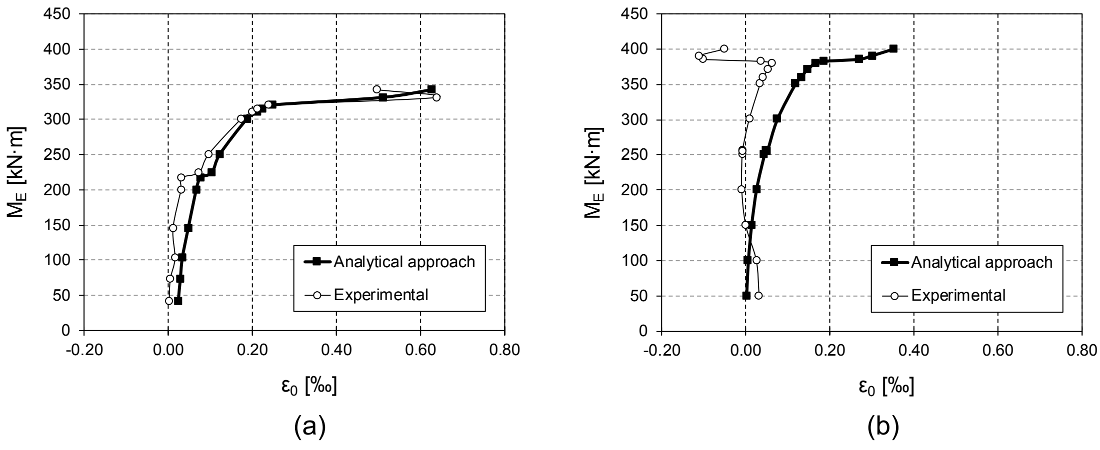

Figure 19: Experimental verification of the analytical model: (a) Specimen V1-20 (Web-flange shear V failure); (b) Specimen V3-0 (Web-flange shear H failure)

4.2.4. Results.

Table 9 shows the results for each specimen. The most significant situations were selected: the maximum resultant axial force situation in flange $N_{f,max}$ and the maximum moment situation supported by beam $M_{E,max}$. Both the results of the resultant compressive force in flange N_f and the compressive forces of the two flanges and central section N_{f2} are provided in the three specimens whose failure occurred by longitudinal shear according to a horizontal surface (V2-0, V3-0 and V2-20). In addition, the moment – curvature diagrams (M_E–χ_E) and the moment – compressive resultant force on the flange (M_E–N_f) of two specimens, whose web-flange longitudinal shear failure was along a vertical plane, are displayed (Figure 20 and Figure 21).

Beam	Situation	M_E (mkN)	b_{ef} (mm)	N_f (kN)	N_{f2} (kN)
V1-0	$N_{f,max}$	240.3	334.2	300.3	-
	$M_{E,max}$	281.2	189.4	254.2	-
V2-0	$N_{f,max}$	374.0	264.7	362.9	837.9
	$M_{E,max}$	379.7	293.9	356.7	809.5
V3-0	$N_{f,max}$	380.3	420.7	515.2	1127.5
	$M_{E,max}$	399.7	352.9	493.3	1089.4
V4-0	$N_{f,max}$	384.9	392.3	504.2	-
	$M_{E,max}$	402.2	359.8	496.4	-
V1-20	$N_{f,max}$	315.0	394.4	429.0	-
	$M_{E,max}$	341.9	284.8	374.2	-
V2-20	$N_{f,max}$	-	-	-	-
	$M_{E,max}$	441.8	421	574.6	1244.2
V3-20	$N_{f,max}$	-	-	-	-
	$M_{E,max}$	518.4	478.1	682.0	-
V1-30	$N_{f,max}$	380.2	338.8	487.2	-
	$M_{E,max}$	410.2	365.4	453.4	-
V2-30	$N_{f,max}$	-	-	-	-
	$M_{E,max}$	475.9	459.1	645.4	-
V3-30	$N_{f,max}$	-	-	-	-
	$M_{E,max}$	497.6	443.7	680.0	-
V1-40	$N_{f,max}$	359.9	482.6	501.9	-
	$M_{E,max}$	371.1	429.1	496.0	-
V2-40	$N_{f,max}$	-	-	-	-
	$M_{E,max}$	398.2	392.9	538.1	-
V3-40	$N_{f,max}$	370.2	472.8	524.9	-
	$M_{E,max}$	372.2	438.1	511.2	-

Table 9: The web-flange longitudinal shear assessment results.

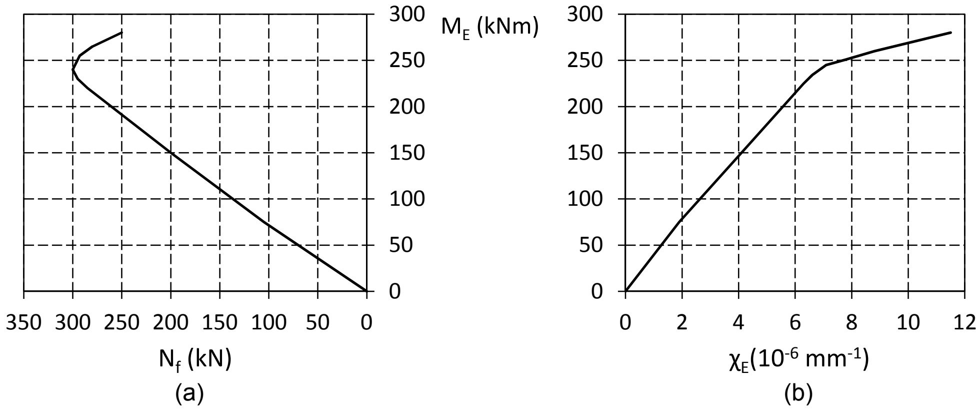

Figure 20: V1-0 specimen: (a) M_E–N_f diagram, (b) M_E–χ_E diagram.

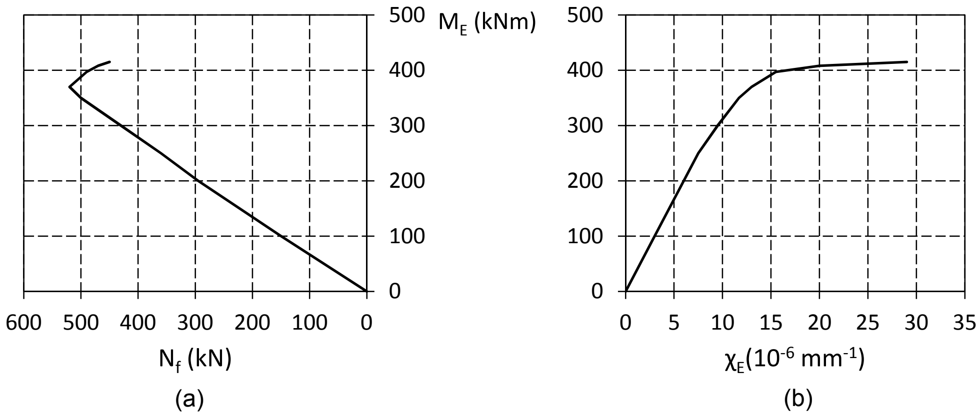

Figure 21: Specimen V1-30: (a) M_E–N_f diagram, (b) M_E–χ_E diagram.

The maximum compressive axial force value in flange N_f was reached before obtaining the maximum load level supported by beam $M_{E,max}$. Specimens V1-0, V1-20 and V1-30 reached the maximum N_f value at a vertical load of 14.5%, 7.9% and 7.3% lower than the maximum vertical load, respectively. This occurred because the web was able to increase the specimen's maximum bearing moment, even though flanges did not transmit more compressive axial force (Figure 20 and Figure 21). Effective width grew when the flange transverse reinforcement ratio was higher as flanges could transmit more compressive axial force before failure occurred.

Figure 22 displays the web-flange normalised shear stress t (Equation (16)) in relation to the flange transverse reinforcement mechanical ratio ω (Equation (18)).

$$t = \frac{\tau_{xy}}{f_c} \tag{16}$$

where:

τ_{xy}: Mean longitudinal shear stress at the web-flange junction.

$$\tau_{xy} = \frac{N_f}{a \cdot h_f} \qquad (17)$$

a: Length between the support and loading point (Figure 15.a).

h_f: Flange thickness (Figure 15).

ω: Flange transverse reinforcement mechanical ratio.

$$\omega = \frac{A_s \cdot f_y}{a \cdot h_f \cdot f_c} \qquad (18)$$

A_s: Flange transverse reinforcement area.

f_y: Steel yield stress.

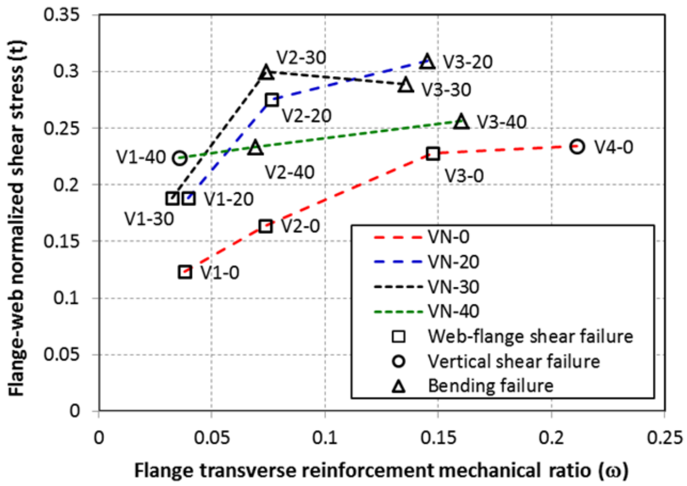

Figure 22: Representation of the experimental results.

Figure 22 confirms the beneficial effect of the presence of steel fibres depending on fibre content. This can be seen with the VN-20 family in relation to the VN-0 fibreless family. The effect diminished in the VN-30 family, which also showed an anomalous result with V3-30. However, it must be pointed out that the representation of failures by another cause other than web-flange shear took a lower web-flange shear strength value. The VN-40 family exhibited irregular behaviour. Beam V1-40 showed poor concrete compaction and hollows. As a result, the failure was concrete crushing for the compression of the strut of the web due to vertical shear. Notwithstanding, the normalised shear stress in the ultimate state of V1-40 beam exceeded the shear resisted by the three beams with an equal flange transverse reinforcement ratio ω and lower fibre content (V1-0, V1-20 and V1-30), which all failed by web-flange shear. On the contrary, the normalised shear stress of beams V2-40 and V3-40 was lower than that of the beams with less fibre content (but exceeded that of the concrete beams without fibres: V2-0 and V3-0). This is due to the concrete of beams V2-40 and V3-40 showed marked porosity on the lateral sides of the web, but did not show visible hollows as in V1-40.

5. Summary and Conclusions.

The conclusions about this experimental campaign of 13 T-beams, made with concrete with and without fibres, are the following:

- Steel fibres improved the longitudinal shear strength in T-beams with a lower transverse reinforcement ratio than that required. Fibre content and the flange transverse reinforcement ratio can determine the failure mode.
- The beam effective width depends on the applied load. A reduction in the effective width was noted as the applied load level increased in the beams with a lower flange transversal reinforcement ratio and with low steel fibre content. This result could be due to the fact that the arranged transverse reinforcement was lower than the minimum required according to Hendy and Smith [69].
- The tested beams went through the following stages in the ultimate state due to web-flange shear: pronounced longitudinal cracking at the web-flange junctions, yielding of flange transverse reinforcements, an increase in the longitudinal strains in the web and a reduced flange effective width.
- A relatively small concrete cover thickness of compressed reinforcements plus a high amount of these stirrups can cause web-flange shear failure along a horizontal plane instead of along a vertical plane at the web-flange junction.
- According to the experimental results, longitudinal shear cracking started on the lower side of the web-flange junction. This behaviour was also observed by Tizatto and Shehata [32].

- Although crack formation followed a double symmetry pattern (transversal and longitudinal symmetry), failure was not symmetrical.
- Effective width practically coincided with the real one for the first load levels, and before web-flange cracking in both the tested and Tizatto beams [20].

The conclusions about cracking web-flange longitudinal shear determination are the following:

- A procedure, based on the model of Regan and Placas [18] y Tizatto [20], has been developed to calculate the load that causes web-flange longitudinal cracking and to determine if a minimum flange transverse reinforcement ratio to resist web-flange longitudinal shear is necessary. A minimum flange transverse reinforcement ratio is needed when the load that causes web-flange longitudinal shear cracking is lower than the theoretical load that would produce beam failure due to either bending or vertical shear. Otherwise, the beam could work perfectly without transverse reinforcement, as long as the high lateral bending in flanges is avoided. The theoretical longitudinal shear cracking load obtained for the tested beams adequately came close to the experimental values.
- It has been analytically justified that longitudinal cracking in the flange starts on the bottom side.

The mean web-flange longitudinal shear determination conclusions are the following:

- The maximum web-flange longitudinal shear situation does not have to coincide with the maximum bending moment situation at the midspan section. The maximum longitudinal shear situation may be reached earlier. In this case, web strength capacity is able to increase the cross section's bearing moment, even though effective width is reduced with increased load.
- The beneficial effect of including fibres in the concrete mass is confirmed. This effect was stronger when including 20 kg/m^3 in relation to fibreless concrete.

Consequently, it is possible to replace transverse reinforcement with steel fibres to resist web-flange shear.

Acknowledgments.

The research presented herein forms part of the research undertaken in the Civil Engineering Department at the Universitat d'Alacant (UA, Spain). The experimental programme was been carried out thanks to the selfless contribution of the Bortubo S.A. company.

References.

[1] Fomento EM de, Hormigón ECP del. EHE-08: Instrucción de Hormigón Estructural : con comentarios de los miembros de la Comisión Permanente del Hormigón. Ministerio de Fomento, Secretaría General Técnica; 2008.

[2] EN 1992-1-1; Eurocode 2: Design of concrete structures - Part 1-1: General rules and rules for buildings. 2004.

[3] Razaqpur AG, Ghali A. Forces at flange-web connections in T-beams. Canadian Journal of Civil Engineering 1984;11:943–54.

[4] CEB-FIB. Fib Model Code for Concrete Structures 2010 (MC2010). Lausanne. International Federation for Structural Concrete: Ernst & Sohn; 2010.

[5] ACI Committee 318. ACI 318-14: Building Code Requirements for Structural Concrete and Commentary. 2014.

[6] American Association of State Highway and Transportation Officials. AASHTO LRFD Bridge Design Specifications. 8th Edition. Washington (DC): 2017.

[7] Canadian Standards Association. CAN/CSA-S6-06: "Canadian Highway Bridge Design Code 2006.

[8] JSCE (Japan Society of Civil Engineers). Standard Specifications for Concrete Structures - 2007. Design. JSCE Guideline for Concrete; 2007.

[9] Canadian Standards Association,, Mississaugua. Design of Concrete Structures, CSA A23.3-04. Canada,: 2004.

[10] A. Koray Tureyen and Robert J. Frosch. Concrete Shear Strength: Another Perspective. Structural Journal 2003;100. doi:10.14359/12802.

[11] Swamy RN, Qureshi SA. An ultimate shear strength theory for reinforced concrete T-beams without web reinforcement. Matériaux et Construction 1974;7:181–9. doi:10.1007/BF02473833.

[12] Kotsovos M, Bobrowski J, Eibl J. BEHAVIOUR OF REINFORCED CONCRETE T-BEAMS IN SHEAR. vol. 65. 1987.

[13] Ioannis P. Zararis MKK and Prodromos D Zararis. Shear Strength of Reinforced Concrete T-Beams. Structural Journal 2006;103. doi:10.14359/16921.

[14] Leonhardt F, précontrainte F internationale de la. Shear and Torsion in Prestressed Concrete. Cement & Concrete Association; 1970.

[15] Alexander Placas and Paul E. Regan. Shear Failure of Reinforced Concrete Beams. Journal Proceedings 1971;68. doi:10.14359/15237.

[16] Kani MW, Huggins MW, Kani G, Wittkopp RR. Kani on shear in reinforced concrete. University of Toronto, Dept. of Civil Engineering; 1979.

[17] Badawy M, Bachmann H. Versuche über Längsschub und Querbiegung in Druckplatten von Betonträgern. Zurich.: Institut für Baustatik and Konstruktion, ETH; 1977.

[18] Regan PA, Placas A. Limit-state design for shear in rectangular and T beams. Magazine of Concrete Research 1970;22:197–208.
[19] Fiorito MT. Cortante longitudinal em vigas de concreto com mesas comprimidas. Universidade Federal do Rio de Janeiro, 1987.
[20] Tizatto V. Estudo Teórico-experimental da resistência ao cortante longitudinal nas mesas comprimidas de vigas de concreto. Universidade Federal do Rio de Janeiro, 1987.
[21] Balaca P, Díaz del Valle J. Armado de las alas de las vigas de sección en T. Hormigón y Acero 1992;184:23–39.
[22] Morley CT, Rajendran S. The strength and effective width of reinforced concrete flanges. Proceedings of the Institution of Civil Engineers 1975:103–22.
[23] Davies C. Tests on half-scale steel-concrete composite beams with welded stud connectors. The Structural Engineer 1969;47.
[24] Ayensa A, Oller E, Beltrán B, Ibarz E, Marí A, Gracia L. Influence of the flanges width and thickness on the shear strength of reinforced concrete beams with T-shaped cross section. Engineering Structures 2019;188:506–18. doi:10.1016/j.engstruct.2019.03.057.
[25] Viktor Sigrist. Generalized Stress Field Approach for Analysis of Beams in Shear. Structural Journal 2011;108. doi:10.14359/51682989.
[26] Frank J. Vecchio and Michael P. Collins. The Modified Compression-Field Theory for Reinforced Concrete Elements Subjected to Shear. Journal Proceedings 1986;83. doi:10.14359/10416.
[27] Schütte B, Sigrist V. Shear assessment of compression flanges of structural concrete T-beams. Frontiers of Structural and Civil Engineering 2014;8:354–61. doi:10.1007/s11709-014-0082-z.
[28] Fausto Minelli and Frank J. Vecchio. Compression Field Modeling of Fiber-Reinforced Concrete Members Under Shear Loading. Structural Journal 2006;103. doi:10.14359/15182.
[29] Conforti A, Minelli F. Compression field modelling of fibre reinforced concrete shear critical deep beams: a numerical study. Materials and Structures 2016;49:3369–83. doi:10.1617/s11527-015-0725-0.
[30] Haoxiong F, Weijian Y. Research on the shear of reinforced concrete T beams based on the MCFT calculation method. IOP Conference Series: Earth and Environmental Science 2018;153:052044. doi:10.1088/1755-1315/153/5/052044.
[31] Zhang F, Ding Y, Xu J, Zhang Y, Zhu W, Shi Y. Shear strength prediction for steel fiber reinforced concrete beams without stirrups. Engineering Structures 2016;127:101–16. doi:10.1016/j.engstruct.2016.08.012.
[32] Tizatto V, Shehata LCD. Longitudinal shear strength of wide compression flanges. Materials and Structures 1990;23:26–34. doi:10.1007/BF02472995.
[33] R. N. Swamy HMB. The Effectiveness of Steel Fibers as Shear Reinforcement. Concrete International 1985;7.
[34] Job Thomas and Ananth Ramaswamy. Shear Strength of Prestressed Concrete T-Beams with Steel Fibers Over Partial/Full Depth. Structural Journal 2006;103. doi:10.14359/15321.
[35] de Montaignac R, Massicotte B, Charron J-P. Design of SFRC structural elements: flexural behaviour prediction. Materials and Structures 2012;45:623–36. doi:10.1617/s11527-011-9785-y.
[36] Abdul-Ahad RB, Aziz OQ. Flexural strength of reinforced concrete T-beams with steel fibers. Cement and Concrete Composites 1999;21:263–8. doi:10.1016/S0958-9465(99)00009-8.
[37] Sahoo DR, Bhagat S, Reddy TCV. Experimental study on shear-span to effective-depth ratio of steel fiber reinforced concrete T-beams. Materials and Structures 2016;49:3815–30. doi:10.1617/s11527-015-0756-6.
[38] Fattuhi Nijad I. Strength of FRC Corbels in Flexure. Journal of Structural Engineering 1994;120:360–77. doi:10.1061/(ASCE)0733-9445(1994)120:2(360).

[39] Campione G. Flexural behaviour of concrete corbels containing steel fibers or wrapped with FRP sheets. Materials and Structures 2005;38:617–25. doi:10.1617/14210.
[40] Giuseppe Campione LLM and Maria Letizia Mangiavillano. Steel Fiber-Reinforced Concrete Corbels: Experimental Behavior and Shear Strength Prediction. Structural Journal 2007;104. doi:10.14359/18859.
[41] Campione G. Performance of Steel Fibrous Reinforced Concrete Corbels Subjected to Vertical and Horizontal Loads. Journal of Structural Engineering 2009;135:519–29. doi:10.1061/(ASCE)0733-9445(2009)135:5(519).
[42] Khosravikia F, Kim H su, Yi Y, Wilson H, Yousefpour H, Hrynyk T, et al. Experimental and Numerical Assessment of Corbels Designed Based on Strut-and-Tie Provisions. Journal of Structural Engineering 2018;144:04018138. doi:10.1061/(ASCE)ST.1943-541X.0002137.
[43] Parol J, Qazweeni J, Salam SA. Analysis of reinforced concrete corbel beams using Strut and Tie models. vol. 21. 2018. doi:10.12989/cac.2018.21.1.095.
[44] Mohamed RN, Elliott KS. Shear strength of short recess precast dapped end beams made of steel fibre self-compacting concrete 2008:11.
[45] Aswin M, Mohammed BS, Liew MS, Syed ZI. Shear Failure of RC Dapped-End Beams. Advances in Materials Science and Engineering 2015;2015:1–11. doi:10.1155/2015/309135.
[46] Ajina J. Effect of steel fibers on precast dapped-end beam connections. South Dakota State University, 1986.
[47] Campione G. Flexural Behavior of Steel Fibrous Reinforced Concrete Deep Beams. vol. 138. 2012. doi:10.1061/(ASCE)ST.1943-541X.0000442.
[48] Moradi M, Esfahani MR. Application of the strut-and-tie method for steel fiber reinforced concrete deep beams. Construction and Building Materials 2017;131:423–37. doi:10.1016/j.conbuildmat.2016.11.042.
[49] Dipti R. Sahoo CAF and Shih-Ho Chao. Behavior of Steel Fiber-Reinforced Concrete Deep Beams with Large Opening. Structural Journal 2012;109. doi:10.14359/51683630.
[50] Romero, MA. Impact of steel fibers in compression strut capacity. University of Nevada, 1994.
[51] Colombo M, di Prisco M, Lamperti M. SFRC D-regions: Size effect in bottle-shaped struts, Chennai, India: BAGNEAUX RILEM Publications S.A.R.L.; 2008.
[52] Zhao J, Li K, Shen F, Zhang X, Si C. An analytical approach to predict shear capacity of steel fiber reinforced concrete coupling beams with small span-depth ratio. Engineering Structures 2018;171:348–61. doi:10.1016/j.engstruct.2018.05.072.
[53] Fehling E, Leutbecher T, Roeder F. Compression-Tension Strength of Reinforced and Fiber-Reinforced Concrete. ACI Structural Journal 2011;108. doi:10.14359/51682351.
[54] Wang DZ. Analysis of Ultra-High Performance Fibre Reinforced Concrete Structures using Truss Models. University of Toronto, 2014.
[55] Schnütgen B, Bochum R-U. Design of precast steel fibre reinforced tunnel elements, Bochum, Germany: 2003, p. 145–52.
[56] López-Juárez JA. Estudio experimental del rasante en vigas en T de hormigón armado reforzado con fibras de acero. Universidad de Alicante, 2016.
[57] Vinayagam, T. Shear transfer in high strength concrete. PhD Thesis. Department of Civil Engineering, National University of Singapore, 2004.
[58] Lee, GG, Foster SJ. Behaviour of steel fiber reinforced mortar in shear I: Direct shear testing 2006.
[59] Wang C. Experimental investigation on behavior of steel fiber reinforced concrete (SFRC). Master thesis. University of Canterbury, 2006.

[60] Al-Sulayvani BJ, Al-Feel JR. Effect of direct compressive stress on the shear transfer strength of fibrous concrete. AL Rafdain Engineering Journal 2009;17:65–75.
[61] Ridha MMS, Hamad NT, Sarsam: KF. Predicting the strength of fiber reinforced high strength performance concrete based on push-off tests. Engineering & Technology Journal 2012;30:1187–202.
[62] Khanlou A, MacRae GA, Scott AN, Hicks SJ, Clifton GC. Shear performance of steel fibre-reinforced concrete, Christchurch, New Zealand: 2013, p. 7.
[63] Domingues LC. Longitudinal shear strength of web-flange junctions in reinforced concrete. Polytechnic of Central London, 1981.
[64] AENOR. Spanish Association for Standards and Certification. UNE-EN 12390-3:2009. Testing hardened concrete - Part 3: Compressive strength of test specimens 2009.
[65] AENOR. Spanish Association for Standards and Certification. UNE-EN 14651:2007. Test method for metallic fibre concrete - Measuring the flexural tensile strength (limit of proportionality (LOP), residual) 2017.
[66] Ferreira L, Gettu R, Bittencourt: T. Study of crack propagation in the specimen recommended by RILEM TC 162-TDF based on Linear Elastic Fracture Mechanics. 2001.
[67] AENOR. Spanish Association for Standards and Certification. UNE-EN ISO 6892-1:2017. Metallic materials. Tensile testing. Part 1: Method of test at ambient temperature. 2002.
[68] EN 1992-2:2005; Eurocode 2. Design of concrete structures - Part 2: Concrete bridges. 2005.
[69] C.R. Hendy, D.A. Smith. Designers' Guide to EN 1992 Eurocode 2: Design of concrete structures. Part 2: concrete bridges. Thomas Telford Ltd; 2007. doi:10.1680/dgte2.31593.
[70] Ministerio de Fomento. EH-91: Instrucción para el proyecto y la ejecución de obras de hormigón en masa o armado. 1991.
[71] Brendel G. Die mitwirkende plattenbreite nach Theorie und Versuch. Beton- Und Stahlbetonbau 1960;8.
[72] Hendy CR, Smith DA. Designers' Guide to EN 1992-2 Eurocode 2: Design of concrete structures. Thomas Telford Publishing; 2007. doi:10.1680/dgte2.31593.
[73] Campione G. Compressive behavior of short fibrous reinforced concrete members with square cross-section. Structural Engineering and Mechanics 2011;37:649–69.